Plasmonic Nanoparticle Modified Substrate for SERS Sensing Applications

by

Gizem Hasibe Kanat

A Dissertation Submitted to the
Graduate School of Sciences and Engineering
in Partial Fulfillment of the Requirements for
the Degree of

Master of Science

in

Chemistry

July 24, 2023

Plasmonic Nanoparticle Modified Substrate for SERS Sensing Applications

Koç University

Graduate School of Sciences and Engineering

This is to certify that I have examined this copy of a master's thesis by

Gizem Hasibe Kanat

and have found that it is complete and satisfactory in all respects,

and that any and all revisions required by the final

examining committee have been made.

Committee Members:

_____

Assoc. Prof. Uğur Ünal (Advisor)

_____

Assist. Prof. Umut Aydemir

_____

Assoc. Prof. Mustafa Kemal Bayazıt

Date: _____

ABSTRACT

Plasmonic Nanoparticle Modified Substrate for SERS Sensing Applications

Gizem Hasibe Kanat

Master of Science in Chemistry

July 24, 2023

Numerous research on the toxicity of N-derived species like nitrite and ammonia have been conducted as a result of their widespread existence in the environment. The ecological system is threatened by nutrient pollution, which is mostly caused by heavy use of fertilizers. Another source of pollution is the industrial gas chimneys and internal combustion engines. Numerous analytical techniques, such as chromatography ,electrochemistry and colorimetry have been developed for the study of nitrite ions in the literature [1]–[3].

Another advantage of developing NO_x and NH_3 detection devices is that they play a role in disease identification. Nitrite and ammonia are biomarkers used to diagnose lung and respiratory disorders, as well as kidney and digestive system diseases .[4]–[6].

Surface-Enhanced Raman scattering (SERS), due to its high sensitivity and resolution, has been extensively researched since its discovery on a rough Ag surface. Up to now, anisotropic noble metal nanostructures (Ag and Au) with tunable absorption bands in a wide spectral range have demonstrated high SERS activity via electromagnetic enhancement mechanism (EM) [7].

This dissertation is concerned with the manufacture of plasmonic metal particle substrates and their application to the detection of N-derived molecules. The first two parts present the synthesis of nanoparticles on copper plates. Ag and Au nanoparticle modified copper films with different morphologies are investigated. The homogeneous distribution of Ag and Au nanoparticles on the Cu surface resulted from successful assembly of nanoparticles and surface characteristics of the used copper plate.

The final section presents the production of nanoparticles on a 3-D graphene oxide framework. Three-dimensional (3D) graphene materials with distinct characteristics have not yet been substantially investigated for SERS applications. Graphene aerogels (GA) with Ag modifications were used as SERS substrates in this research.

SERS performance of substrates were examined by detecting an N-derived probe molecule; Rhodamine B (RhB). The highest-sensitivity substrate is then used for nitrite detection.

The detection limit for RhB molecules is 10^{-8} M for Ag NPs modified Cu substrate, 10^{-16} M for Au-Ag NPs modified substrate, and 10^{-6} for Ag NPs modified GA substrate. The SERRS technique (Surface Enhanced Resonance Raman Spectroscopy) was used to study nitrite detection adopting azo dye production. The most promising substrate could achieve detecting nitrite concentrations as low as 10^{-14}M.

ÖZETÇE

SERS Algılama Uygulamaları için Plazmonik Nanoparçacık Modifiyeli Substrat

Gizem Hasibe Kanat

Kimya, Yüksek Lisans

24 Temmuz, 2023

Nitrit ve amonyak gibi N-türevi türlerin toksisitesi üzerine, çevrede yaygın olarak bulunmalarının bir sonucu olarak çok sayıda araştırma yapılmıştır. Ekolojik sistem, çoğunlukla yoğun gübre kullanımından kaynaklanan besin kirliliği nedeniyle tehdit altındadır. Bir diğer kirlilik kaynağı da endüstriyel gaz bacaları ve içten yanmalı motorlardır. Literatürde nitrit iyonlarının incelenmesi için kromatografi, elektrokimya ve kolorimetri gibi çok sayıda analitik teknik geliştirilmiştir [1]–[3].

NOx ve NH3 tespit cihazlarının geliştirilmesinin bir diğer avantajı da hastalık tespitinde etkin rol almalarıdır. Nitrit ve amonyak, akciğer ve solunum bozukluklarının yanı sıra böbrek ve sindirim sistemi hastalıklarının teşhisinde kullanılan biyobelirteçlerdir [4]-[6].

Yüzey Destekli Raman saçılması (SERS), yüksek hassasiyeti ve çözünürlüğü nedeniyle, pürüzlü bir Ag yüzeyinde keşfedilmesinden bu yana kapsamlı bir şekilde araştırılmıştır. Şimdiye kadar, geniş bir spektral aralıkta ayarlanabilir absorpsiyon bantlarına sahip anizotropik soy metal nanoyapılar (Ag ve Au), elektromanyetik güçlendirme mekanizması (EM) aracılığıyla yüksek SERS aktivitesi göstermiştir [7].

Bu tez, plazmonik metal parçacık substratlarının üretimi ve bunların N türevi moleküllerin tespitine uygulanması ile ilgilenmektedir. İlk iki bölüm, bakır plakalar üzerinde nanoparçacıkların sentezini sunmaktadır. Farklı morfolojilere sahip Ag ve Au nanoparçacık modifiye bakır filmler incelenmiştir. Ag ve Au nanoparçacıklarının Cu yüzeyindeki homojen dağılımı, nanoparçacıkların başarılı bir şekilde bir araya getirilmesinden ve kullanılan bakır plakanın yüzey özelliklerinden kaynaklanmaktadır.

Son bölümde 3 boyutlu grafen oksit iskelet üzerinde nanoparçacık üretimi sunulmaktadır. Farklı özelliklere sahip üç boyutlu (3D) grafen malzemeler SERS uygulamaları için henüz önemli ölçüde araştırılmamıştır. Bu araştırmada Ag modifikasyonlu grafen aerojeller (GA) SERS substratları olarak kullanılmıştır.

Substratların SERS performansı, N türevi bir prob molekülü olan Rhodamine B (RhB) tespit edilerek incelenmiştir. En yüksek hassasiyete sahip substrat daha sonra nitrit tespiti için kullanılmıştır.

RhB molekülleri için tespit limiti Ag nanoparçacık modifiye Cu substrat için 10^{-8} M, Au-Ag nanoparçacık modifiye substrat için 10^{-16} M ve Ag nanoparçacık modifiye GA substrat için 10^{-6}'dır. SERRS tekniği (Yüzey Geliştirilmiş Rezonans Raman Spektroskopisi), azo boya üretimini benimseyen nitrit tespitini incelemek için kullanılmıştır. En başarılı substrat 10^{-14}M kadar düşük nitrit konsantrasyonlarını tespit edebilmiştir.

ACKNOWLEDGEMENTS

Firstly, I would like to thank my supervisor Assoc. Prof. Uğur Ünal for his invaluable support and guidance I have received throughout my journey of masters. I gained a lot from his expertise and knowledge in research, as well as from his positive character, which greatly influenced my learning and personal growth.

Additionally, I want to extend my sincere gratitude to my jury members. Assoc. Prof. Umut Aydemir and Assoc. Prof. Mustafa Kemal Bayazıt for taking their time to evaluate my work and providing valuable feedback.

I want to express my appreciation to Dr. Mohammadreza Khobadaskh for his help and mentorship. The research we undertook together was profoundly influenced by his guidance. I want to thank my lab mates Bengisu Yılmaz, Armin Asghari Alamdari, Tuğba Yalçın, Hossein Mahdavi, Ceren Ünver, M. Tuğrul Avcu. I am grateful for the vibrant and supportive environment.

I would like to thank the KUYTAM (Koç University Surface Science and Technology Center) researchers for their assistance. Dr. M. Barış Yağcı for the XPS and SEM analyses. Dr. Gülsu Şimşek Franci and Dr. Hadi Jahangiri for their trainings and help.

This project was supported by the Nanosis platform titled Integrated, Scalable, Functional Nanostructures and Systems under TUBITAK (Scientific and Technological Research Council of Turkey) 1004 Excellence support programme. I would like to thank Tubitak and the project coordinator SUNUM (Sabancı University Nanotechnology Research and Application Center) for their support.

TABLE OF CONTENTS

LIST OF FIGURES

ABBREVIATIONS

1-NA	1-Naphtylamine
4-ATP	4-Aminothiophenol
CM	Chemical enhancement mechanism
EDTA	Ethylene diamine tetraacetic acid
EF	Enhancement factor
EM	Electromagnetic enhancement mechanism
FESEM	Field Emission Scanning Electron Microscopy
GA	Graphene aerogel
GO	Graphene oxide
LOD	Limit of detection
LSPR	Localized Surface plasmon resonance
NPs	Nanoparticles
RhB	Rhodamine B
RS	Raman Spectroscopy
SERS	Surface Enhanced Raman Spectroscopy
SERRS	Surface Enhanced Resonance Raman Spectroscopy
SPR	Surface plasmon resonance
XPS	X-ray Photoelectron Spectroscopy

Chapter 1:
INTRODUCTION

1.1 Sensing

Sensing has grown significantly in importance for analyte marker analysis in chemical, biological, safety, therapeutic, environmental, and other related sectors in the recent, fast expanding globe. Fast examination and trace recognition have been found to be crucial for detecting chemical and biological species in human-related fields including medicine, food, drug testing, safety, etc. High sensitivity, repeatability and cost-effectiveness appreciated to complete qualified research operations [8]. For the purpose of identifying chemicals, spectroscopy, chromatography, fluorescence and electrochemistry have all been suggested as common procedures to date. Additionally, advanced characterization techniques that offer detailed insights include gas and liquid chromatography, mass spectrometry, infrared or UV-Vis absorption spectroscopy, nuclear magnetic resonance spectroscopy, Raman spectroscopy and colorimetric methods allow for the detection of substances with low detection limits [9], [10], [11].

1.2 Nitrite detection

Toxic gases that accumulate in the atmosphere have been an environmental concern worldwide over the years. NO_x and NH_3 are the two primary pollutants commonly observed among these gases. Internal combustion engines and industrial gas chimneys are the two most significant sources of NO_x-derived gases. The increase in the number of such gases in the atmosphere has detrimental implications, such as global warming and acid rain. NH_3 is produced by ammonia sources utilized in agriculture and some chemical industries. Thus, the identification of nitrogen-derived compounds such as NH_3 and NO_x in the air is critical because they endanger human and environmental health.

Nitrogen-derived molecule detection is also essential for disease identification. Many diseases cause the human body to produce certain chemicals. These chemicals can be identified using various methods to detect disease. NO_2 and NH_3 are released in the human body, presence of some detrimental diseases. Distinct illnesses result in distinct body secretions. For example, NO_x-derived compounds are identified in the breath of

people suffering from lung and respiratory disorders such as asthma [4]–[6]. Even in the early stages of the condition, it is possible to diagnose by measuring the amount of nitrite in the patient's breath. Kidney or digestive system disorders, on the other hand, cause considerable amounts of amine-derived compounds, particularly ammonia and alkyl amines, to emerge in the breath. These amine derivatives chemicals are a type of chemical that is commonly seen as a result of kidney illness, liver disease, or bacterial infections such as H. Pylori [6], [12], [13]. Thus, detecting and monitoring NH_3 and NO_x is essential for the early diagnosis of diseases and for ensuring people's quality of life, and preventing environmental pollution.

1.3 Raman Spectroscopy

Raman spectroscopy (RS), which originates from C.V. Raman's discovery of inelastic scattering, offers a powerful method for obtaining unique vibrational information and serves as a nondestructive technique for accurate substance identification. Unlike absorption-based IR spectroscopy, RS is based on scattering phenomena, providing substantial flexibility in instrument design and sample manipulation [14].

Raman measurements are also very flexible, quick, and easy. Any given material, whether liquid or solid, organic, or inorganic, crystalline or amorphous, can be measured without any prior preparation.

One of the primary techniques used to acquire information about the lattice vibration frequencies of a crystal is through the measurement of its Raman spectrum. The fundamental understanding of the Raman effect has been established for a considerable duration Specifically, incident light with an angular frequency (ωi) has the capability to interact with the crystal, resulting in the creation or elimination of one or more phonons (lattice vibration quanta). The energy exchange, ($\pm\hbar\omega$), experienced by the lattice is offset by a corresponding frequency shift, ($\omega s = \omega i \pm \omega$), of the scattered light (ωs) [15].

Raman spectroscopy is an effective technique for characterizing materials because of the high information content of Raman spectra. The development of micro-Raman techniques that enable the characterization of small amounts of materials and/or small regions within a material. Raman spectroscopy provides molecule-specific data, which is a significant benefit over frequently used detection methods (such UV-visible). As Raman

instrumentation has become easier to use, it has been adopted as a detection mechanism in a wide range of separation techniques [11].

Raman spectroscopy is a rapid and non-destructive technique that allows for the examination of various aspects of a material system, including crystal structure, electronic structure, phonon dispersion, and electron-phonon interaction. When applied to 2D materials, Raman scattering provides valuable structural insights through parameters such as peak frequency, peak intensity, and full width at half maximum (FWHM). These characteristics offer rich information about the material, including layer number, edge chirality, lattice orientation, defect presence, doping levels, strain effects, alloy composition, isotope concentration, and more [16].

1.3.1 Raman Scattering

There are typically three distinct steps in the Raman scattering process in materials. A photon is first absorbed by an electron, which causes it to change from its ground state to a virtual state. The electron is then undergoes to inelastic scattering by one or more phonons. Finally, the electron relaxes back to the ground state, emitting a photon in the process. During Raman scattering, there exists an energy difference between the absorbed and emitted photons, referred to as the Raman shift. As illustrated in Figure 1-1, when the emitted photon has more energy than the absorbed photon, anti-Stokes scattering occurs; when the emitted photon has less energy, Stokes scattering happens.

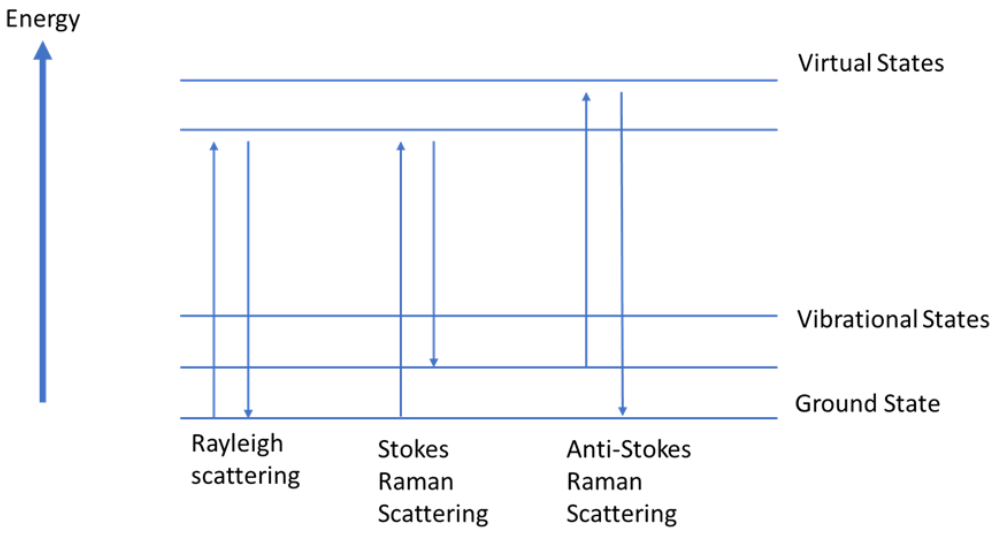

Figure 1-1: Schematic diagram of the energy transitions.

The electron is scattered by a single phonon in the case of first-order Raman scattering. The scattering of two or more phonons causes second- and higher-order Raman peaks, which offer extensive information on the coupling between electrons and phonons in materials. [15], [16]

A localized molecule vibration must be accompanied with a change in polarizability, or a distortion of the electron density, in order to produce a Raman band. In contrast to localized vibrations of singly bound or electron-poor groups, those of multiply bonded or electron-rich groups (such as C=O, C=N, C=C, SS, SC, and SH) typically yield more strong Raman bands.

1.3.2 Raman Instrumentation

Scattered light is investigated by Raman spectrometer. Light changes frequency and color during the scattering process although it is not visible to the naked eye. It is caused by the loss of energy during the interaction with matter, which causes molecular vibrations. Because the Raman effect is relatively weak, it is analyzed by highly sensitive spectrometers.

A Raman spectrometer, as displayed in the Figure 1-2, consist of different components. Single colored lasers are used as a light source with wavelengths ranging from 244 nm to1064 nm. Choice of the wavelength of laser depends on the material and application. Lenses are used to focus the light on the sample and collect the scattered light. High confocal lenses to long working distance lenses(100x,50x,20x) can be used on the sample. And then filters aimed to collect only the Raman light. Another component is the gratings or prisms which provide dispersion and longevity. To detect light, sensitive detectors such as charge coupled devices (CCD) or photomultiplier tubes (PMTs) are used. Detectors convert the incoming light into the electrical signals. A computer is utilized to control the Raman spectrometer equipment and to obtain the spectrum. With the combination of these components, weak Raman scattered light cand be analyzed and the outcomes can be applied in various fields such as chemistry, material science or biology [17].

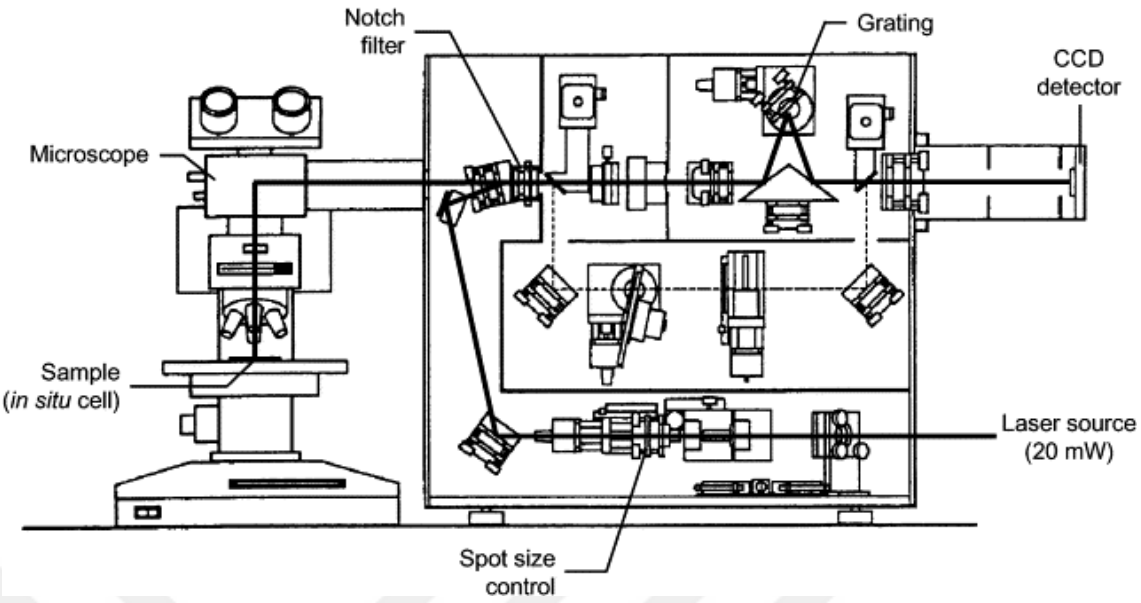

Figure 1-2: General drawing of the Raman imaging microscope [18].

1.3.3 Surface Enhanced Raman Spectroscopy

The most active area of Raman research over the past few years has undoubtedly been SERS (Surface-enhanced Raman spectroscopy). Two recent advances in surface-enhanced Raman spectroscopy have made a particularly big difference. The discovery of extraordinarily high enhancement factors and the ability to detect single molecules by various research groups has significantly heightened the potential of SERS to become the favored method for ultrasensitive detection. The discovery that transition metal thin films devoid of pinholes can be employed as SERS substrates on top of a SERS-active surface is a second advancement with potentially broad-reaching implications. This is a significant finding since it opens up the possibility of studying a number of new surfaces, including those crucial to heterogeneous catalysis.[11]

Surface-enhanced Raman spectroscopy is an exceptionally sensitive method that amplifies the Raman scattering of molecules using nanostructured materials as a support. This technique enables the structural identification of analytes present in low concentrations by utilizing plasmon-mediated amplification of electrical fields or chemical enhancement. Due to its exceptional sensitivity and selectivity, SERS finds extensive applications across a wide range of fields, including surface and interface chemistry, catalysis, nanotechnology, biology, biomedicine, food science, environmental analysis, and various other domains [19], [20].

The pioneering work of Martin Fleischmann in 1974 can be credited with the discovery of SERS. Raman spectroscopy was used by Fleischmann and his team to examine the behavior of pyridine molecules adsorbed on roughened silver electrodes. When the pyridine molecules came into contact with the silver surface, their Raman signals became unusually intense, and they assumed that the surface-area effect was responsible for the enhancement [21].

Later, in 1977, the phenomena was separately recognized by Jeanmaire and Van Duyne[22] and Albrecht and Creighton [23]. Jeanmaire and Van Duyne found that two enhancement processes contribute to the significant increase in Raman intensity observed in Surface Enhanced Raman Spectroscopy. These are the surface enhancement effect and the resonance enhancement effect due to the coupling of the scattering process with an electronic transition in the adsorbed molecule. They also reported peak intensities that were 5-6 orders of magnitude higher than expected. Albrecht and Creighton explained this effect with expanded on Philpott's proposal, suggesting a resonant Raman effect involving plasmon excitation. In 1975 Philpott proposed that broadened electronic energy levels of molecules on roughened metal surfaces could induce resonant Raman scattering through interaction with surface plasmons. [24]

Raman scattering is a rather inefficient process; hence it needs an improvement method to be useful. The synergy between two components, namely electromagnetic (EM) enhancement and chemical (CE) enhancement, gives rise to the overall enhancement factor (EF) observed in SERS. The EM enhancement originates from the excitation of plasmons in metal particles, while the CE enhancement occurs when the target molecules can exchange electrons with the metal particles in both their ground and excited states, often as a result of the formation of metal-molecule bonds.[19], [25], [26] The low cross section of Raman chemical signals is often overcome by substantial amplification, especially in nanostructured metals. Silver (Ag), gold (Au), and copper (Cu) are frequently utilized metals due to their strong plasmonic characteristics and high SERS enhancement factors. However, a crucial challenge in developing highly sensitive SERS substrates lies in creating nanoscale hotspots, which are confined regions with intensified electromagnetic fields. This entails creating small gaps between metal nanoparticles to achieve dense concentrations of electromagnetic energy. Additionally, the nanoparticle structure also contributes to hotspot formation, as geometries featuring sharp nanoscale corners and edges further enhance the electromagnetic energy.[25], [26].

The "lightning rod effect" is a term used to describe the field enhancement that occurs after a strong potential gradient because of the curvature of a metallic interface [27]. Therefore, shape, size and interparticle space of the nanoparticles effects the results. As a result, when designing the new SERS substrates, all the parameters must be carefully chosen.

1.4 Plasmonic Nanoparticles

The surface plasmon resonance (SPR) phenomenon, which is the interaction of a metal NP's conduction electrons with external electromagnetic fields, is related to the optical properties. The size, shape, and other intrinsic geometrical characteristics of the NP, as well as external characteristics like the refractive index of the surrounding medium, have a significant impact on the resulting SPR [28]. The localized surface plasmon resonances (LSPRs) of noble metal nanoparticles, such as those of Au and Ag, are most frequently linked to electromagnetic enhancement [29].

Silver and gold nanoparticles are the most preferred plasmonic materials for SERS applications due to their high enhancement factor, strong air stability, and low reactivity. Bhunia et al. fabricated Carbon dot / silver nanoparticle films for SERS and studied on the bacteria detection [30]. Zhou et al. combined Ag nanoparticles and graphene and investigated the effects of nanoparticle size on SERS performance [31]. Guo et al. used both gold and silver nanoparticles to create a highly sensitive SERS sensor with low detection limits [32]. As stated by Starowicz et al., silver is more cost-effective and has a higher enhancement value than gold, while gold is more stable and inert. Furthermore, the electric field increasement for gold spheres is substantially weaker when compared to silver spheres, as supported by this thesis dissertation. [33].

As depicted in Figure 1-3, metallic NPs can be synthesized via physical methods such as ball milling, laser ablation, and vapor deposition, as well as chemical methods such as chemical reduction, electrochemical, photochemical, and sonochemical

processes. Biological approaches such as bacteria-mediated and plant-mediated methods are also known [34].

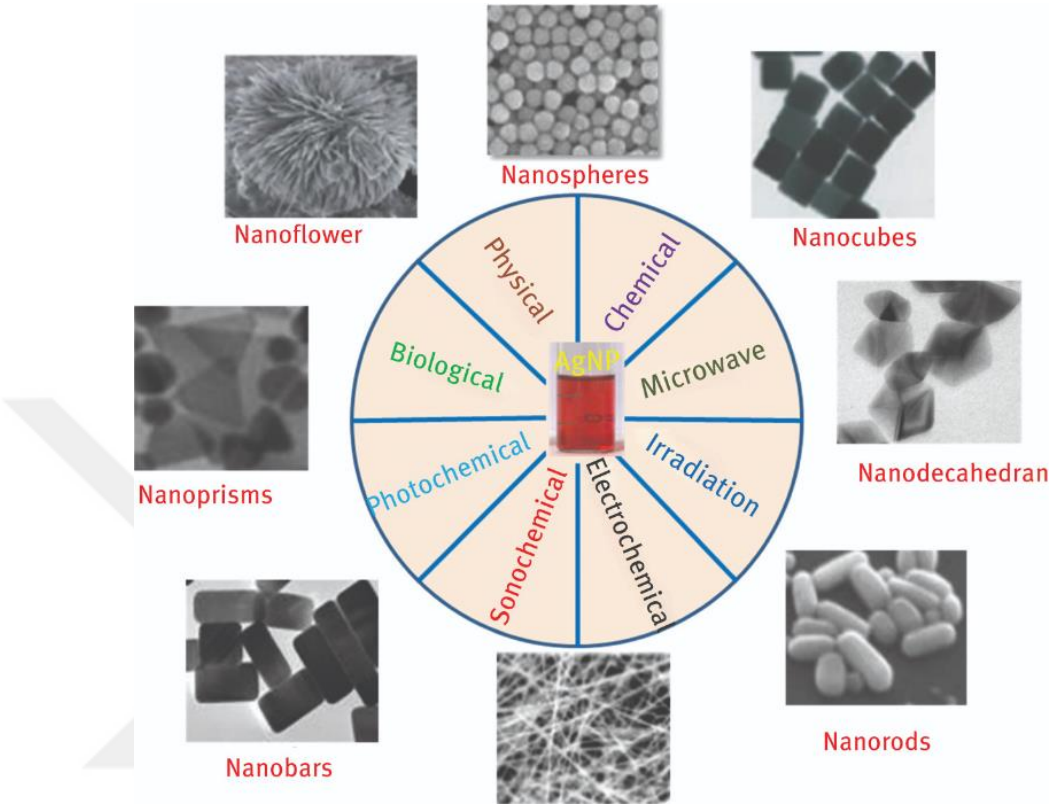

Figure 1-3: Silver nanoparticles with obtained various synthesis methods and shapes are demonstrated [34].

Chemical reduction processes are well established, and shape and size of nanoparticles can be regulated. Various compounds are often included in the formulation as a precursor salt, reducing agent, and stabilizing/capping agent. The majority of bottom-up methods lead to the synthesis of spherical NPs. However, there is currently a lot of interest in shape-controlled synthesis, and scientists have successfully used chemical and photochemical methods to synthesize NPs with a different geometries. [35]–[37].

Chapter 2:
SERS SUBSTRATE: SILVER NANOPARTICLE DECORATED COPPER

2.1 Introduction

To date, spectrophotometry, chromatography, electrochemistry have been proposed as typical approaches for detecting nitrogen-derived compounds in the environment. Advanced characterization technologies such as gas chromatography, mass spectroscopy, infrared or UV-Vis absorption spectroscopy, nuclear magnetic resonance spectrometer and colorimetric methods enable detection of compounds with low detection limits [9], [10]. In the field of medicine, breath or body fluids are utilized to identify N-based compounds. Kidney and respiratory diseases release significant amount of NH_3 and NO_x gases through breath, respectively, thus utilizing human breath for the detection of diseases is one of the applicable and fast method that allows real time detection. In the early 1970s, Pauling et al. employed gas chromatography to detect compounds in human breath [6], [38]–[40]. Chromatography can be used to identify nitrite, but it is expensive and unsuitable for routine nitrite monitoring in the field [1]. Moreover, the change of optical, electrochemical, electrical, and spectroscopic properties of indicators used for detection purposes. Sensors based on electrochemical detection exhibit significant noise levels and low sensitivity [1]. Chemiresistive sensors are commonly used; when the chemicals being analyzed react with the material of the sensor, which is often semi-conductors or conductive polymers, the sensor's resistivity changes. Chemiresistive sensors can be employed for the NH_3 gas detection because NH_3 alters conductivity of semi-conductor materials and create a response. Chemiresistive sensors are easy the manufacture, gives fast response, and has high sensitivity however, they require high temperatures, periodic calibration maintenance and have selectivity issues [40], [41]. The creation of inexpensive, quick, portable, and user-friendly sensors is a current focus. Optical detection of molecules was preferred in this study.

Surface Enhanced Raman Spectroscopy is a frequently used optical approach for detecting molecules. SERS devices, in contrast to colorimetric, electrochemical, and fluorescent sensors, identify the molecular spectral fingerprints of analytes and/or convert the sensing signal by directly obtaining the analyte's SERS spectrum [1]. Because of its

selectivity, exceedingly high sensitivity, and fingerprint effects, SERS has been chosen for detection of compounds in extremely low concentrations. Specifically, the integration of organic reagents in SERS-based devices is particularly suited for applications aimed at the detection of small inorganic compounds with small Raman cross-sections and frequently poor affinity toward the metal surfaces [42]. The Raman signals increase in very high orders as a result of the local electromagnetic field that is created on the metal nanoparticles when they contact with the Raman spectrometer laser. In this manner, even single-molecule identification might be feasible [19].

In this chapter, Ag nanoparticle deposited Cu substrates were prepared via simple and rapid method and readily used as a reliable SERS detection substrate. SERS performance is evaluated using an N-group probe molecule. The morphologies and performances of substrates were compared, and optimum ones were chosen for subsequent applications.

2.2 Materials and Methods

2.2.1 Materials

All the chemicals were used as received without further purification. Polycrystalline Cu foil (25 μm thick, > 99.99%, MTI corporation), silver nitrate ($AgNO_3$, Sigma-Aldrich), ethylene diamine tetraacetic acid (EDTA, Sigma-Aldrich), stannous chloride ($SnCl_2$, Sigma-Aldrich), Rhodamine B (RhB, Alfa Aesar), All solutions are prepared with distilled water.

2.2.2 Synthesis of Ag modified Cu substrates

At the beginning of the experiment, square pieces of Cu plates were cut into 2x2 cm pieces. To remove any organic impurities, the plates were underwent ultrasonic washing with acetone and ethanol each for 2 minutes, subsequently washed with 1% (wt% in water) sulfuric acid for 4 minutes and remaining acid suspended with distilled water. After cleaning the Cu plates, they were immersed into to 1.5 mM $SnCl_2$ for 10 minutes to adsorb stannous ions onto their surface. The plates were then washed with deionized water. The cleaned Cu plates were then immersed in a mixture of 5 mL $AgNO_3$ (3 mM) and 5 mL EDTA (3 mM). The surface of the Cu plates were gradually formed diverse

morphologies of Ag NPs throughout different timeframes of immersion in silver salt EDTA mixture. 5-minutes, 10-minutes, 20-minutes and 3 times 5 minutes immersion times were studied. Afterward, substrates were rinsed with DI water and dried by nitrogen gas Substrate obtained following continuous 20-minute immersion and intermediate 5 minutes x 3 intervals immersion named Ag/Cu and flowerlike-Ag/Cu, respectively.

2.2.3 Preparation of RhB stock solution

Rhodamine B was prepared by dilution of the stock solution with distilled water up to 10^{-14} M. Prepared stock solutions were kept in a dark and cold place.

2.2.4 Structural characterization of Silver modified Cu substrates

Surface chemical structure of the films were analyzed with X-ray photoelectron spectroscopy (XPS, Thermo K-Alpha) with Al Kα source. The fittings for the experimental data were done with Avantage software. Morphology of the NP deposited films were investigated with Field Emission Scanning Electron Microscopy (FESEM, Zeiss Ultra Plus).

2.2.5 Detection of RhB by SERS using NP modified Cu substrates

Raman spectra were recorded using Raman microscope (Renishaw Invia) with 50X objective lens (NA=0.75) with 2.72 mW laser power. For RhB spectra 633 nm laser was used. For each measurement 10 spectra were collected from different spots on the sample to ensure the repeatability. Spot size on the sample refers to the area or size of the laser beam that is focused on the sample is 2.5 μm. SERS substrates were immersed in 0.5 mL Rhodamine B solution for 6 hours prior to Raman detection. Then substrates were dried naturally.

2.3 Results and Discussion

2.3.1 Structural characterization of substrates

As shown in Figure 2-1 in order to synthesize the SERS substrate, the Cu plate was first immersed in the reducing agent ($SnCl_2$) and Sn^{+2} ions were absorbed on the surface. A sample equation is given as [43] ;

$$Sn^{2+} \rightarrow Sn^{4+} + 2e^{-} \quad (2.1)$$

$$2Ag^{+} + 2e^{-} \rightarrow 2Ag^{0} \quad (2.2)$$

$$Sn^{2+} + 2Ag^{+} \rightarrow Sn^{4+} + 2Ag^{0} \quad (2.3)$$

Absorbed Sn^{+2} ions were acted as attachment sites for Ag^{+} ions, which were then reduced to Ag^{0} ions. Through the process, more clumping in the Ag particles resulted in the development of bigger clusters. As a result, Ag nanoparticles were generated on the surface. The FESEM images are displayed in Figure 2-2. According to the figures it was observed that FESEM images were confirmed the silver nanoparticle formation on the Cu plate.

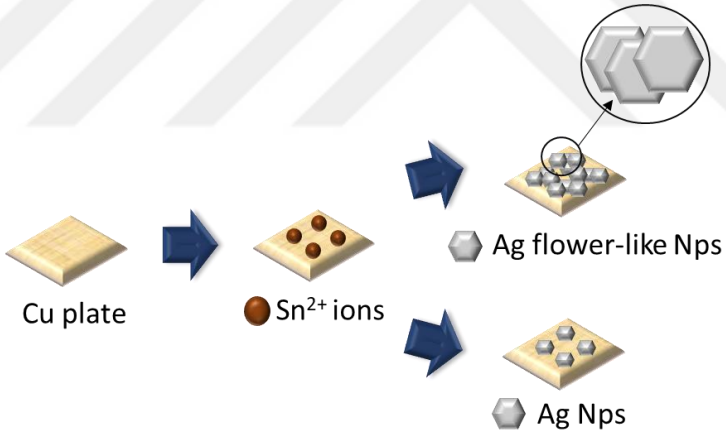

Figure 2-1: The synthesis of Ag NPs/Cu SERS substrate is shown schematically.

As a capping agent, EDTA was used in the synthesis of Ag nanoparticles. Capping agents have a stabilizing effect and inhibits the agglomeration of nanoparticles with increased nucleation. Figure 2-2 demonstrates that the size of metal particles on EDTA-capped samples is small and the size distribution is narrow. The capping agent influences not only the size but also the shape of the nanoparticles. They can bind to different crystallographic surfaces and change their growth rates [44]–[46]. Where EDTA was not attached, the particle expanded in that directions to create a nanoparticle.

The investigation of increasing silver salt immersion times of 5 minutes, 10 minutes, 20 minutes, and 30 minutes are depicted in Figure 2-2. Longer immersion times were resulted in larger Ag nanoparticle sizes, and the shape of Ag nanoparticles were changed. After 20 minutes of reaction time, the Ag nanoparticles were lost their sharp nanoscale tips and tended to become denser. This shape reduces SERS performance due to lower electromagnetic energy caused by the loss of sharp nanoscale corners and edges. It has been demonstrated that areas with significant radius of curvature (sharp tips/edges) are where localized electromagnetic fields are most powerful. The electromagnetic enhancement mechanism was discovered to be the most effective mechanism on SERS behavior. Fan et al. studied effects of different shaped Ag nanoparticles on SERS performance. They stated that when compared to spherical particles, Ag nanoparticles in the form of nanocubes and octahedra produce stronger SERS signals, with Ag octahedra producing the strongest SERS signals. They observed that the enhancement factors of nanocubes are eight times greater than those of spherical particles [29].

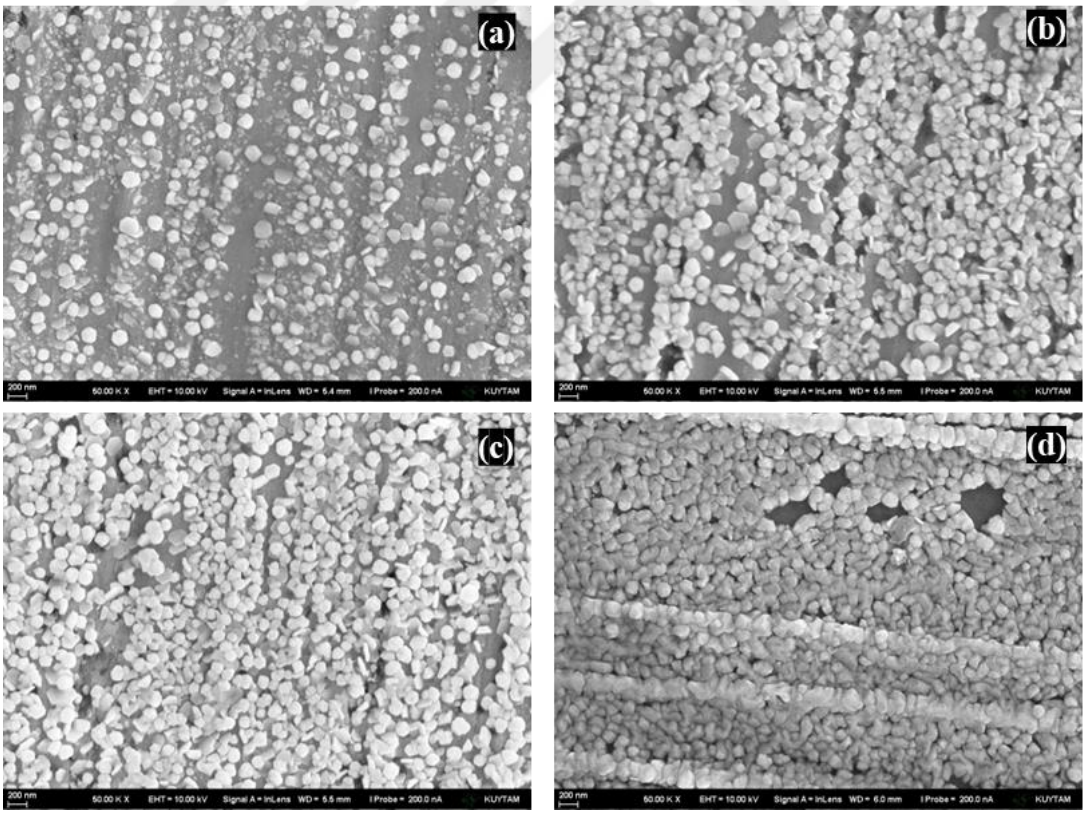

Figure 2-2:SEM image of silver nanoparticles grown on Cu plate for 5, 10, 20 and 30 minutes (a-b-c-d, respectively).

Copper foil was utilized as a substrate because it is inexpensive and provides a flexible substrate with a weak and featureless background signal in SERS. Copper is

mentioned in the literature as an alternative to noble metals. It is known as a SERS-active substrate and is used because of its low toxicity, excellent optical properties, and conductivity. Pereira et al. investigated copper nanostructures and their SERS properties, obtaining remarkable enhancement factors ranging from 10^7 to 10^8 [47]. The optical and SEM image of an empty copper plate, and SEM image of a particle covered copper plate displayed in Figure 2-3. It shows that on the surface of Cu plate there are lines in parallel series produced from its polishing process, called striation. The foil's striation direction offers an ideal setting for the growth and nucleation of silver nanoparticles. Figure 2-3(c-d) shows that the nanoparticles grew in accordance with the foil's surface lines, which helped the nanoparticle deposition process and created well-ordered nanostructures. It enabled in the uniform distribution of nanoparticles, prevented random agglomeration, and promoted more hot spots on the surface.

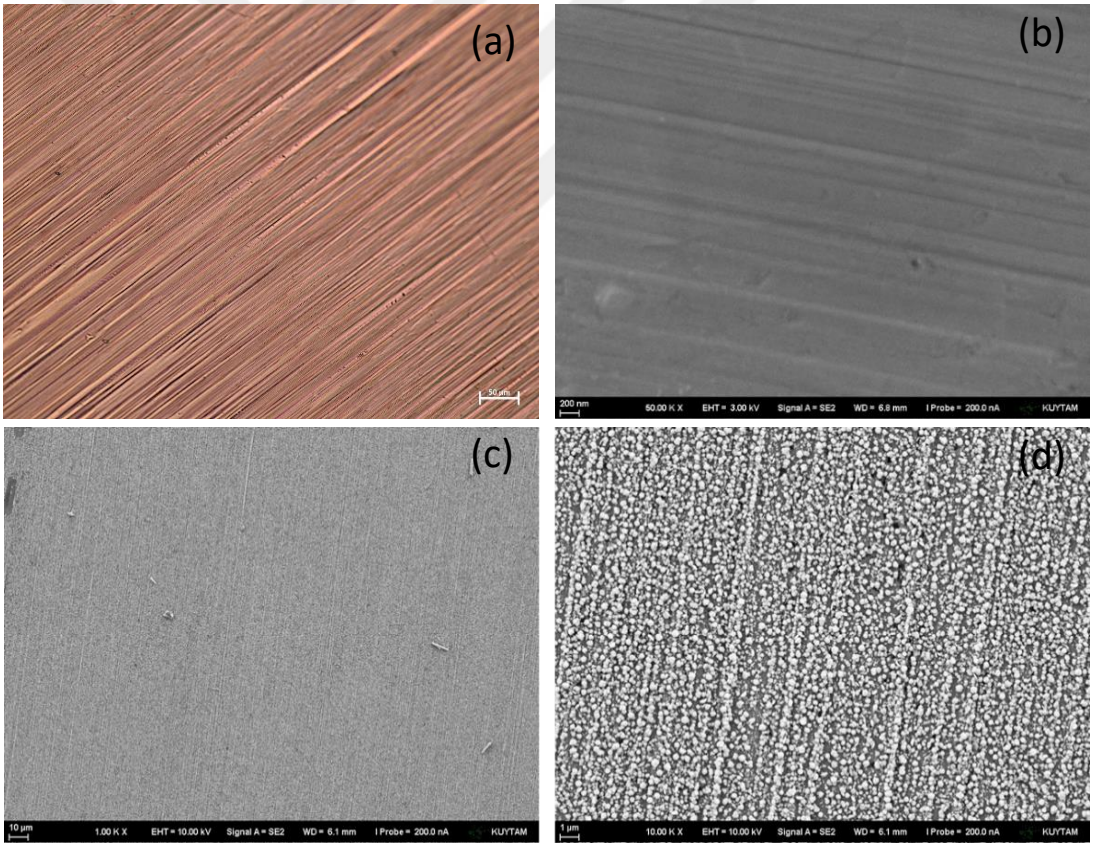

Figure 2-3: (a) Optical image of copper plate (b) SEM image of copper plate (c-d) Silver nanoparticle deposited copper plate

Well-ordered nanostructures are typically possible through time-consuming synthesis and self-assembly procedures, or through expensive patterning techniques like e-beam lithography [48]. Macias et al. studied surface roughness effects of the SERS performance

and they concluded that rough arrays exhibits greater values of the electric field intensity and hot spot densities compared to smooth ones [49]. Tang et al. created wrinkled patterned structures by releasing the flexible polymeric surface after straining. They generated hot spots on the sharp edges and obtained high electromagnetic field enhancements [48]. By combining literature and our findings, we may conclude that striations on the Cu plate provide sufficient roughness for EM enhancement while also assisting in the maintenance of well-ordered nanoparticles on the surface.

Figure 2-4 demonstrates two types of substrates; (a-b) Ag/Cu (c-d) flowerlike-Ag/Cu. Substrates with two different morphologies were examined further for molecule detection using Raman spectroscopy.

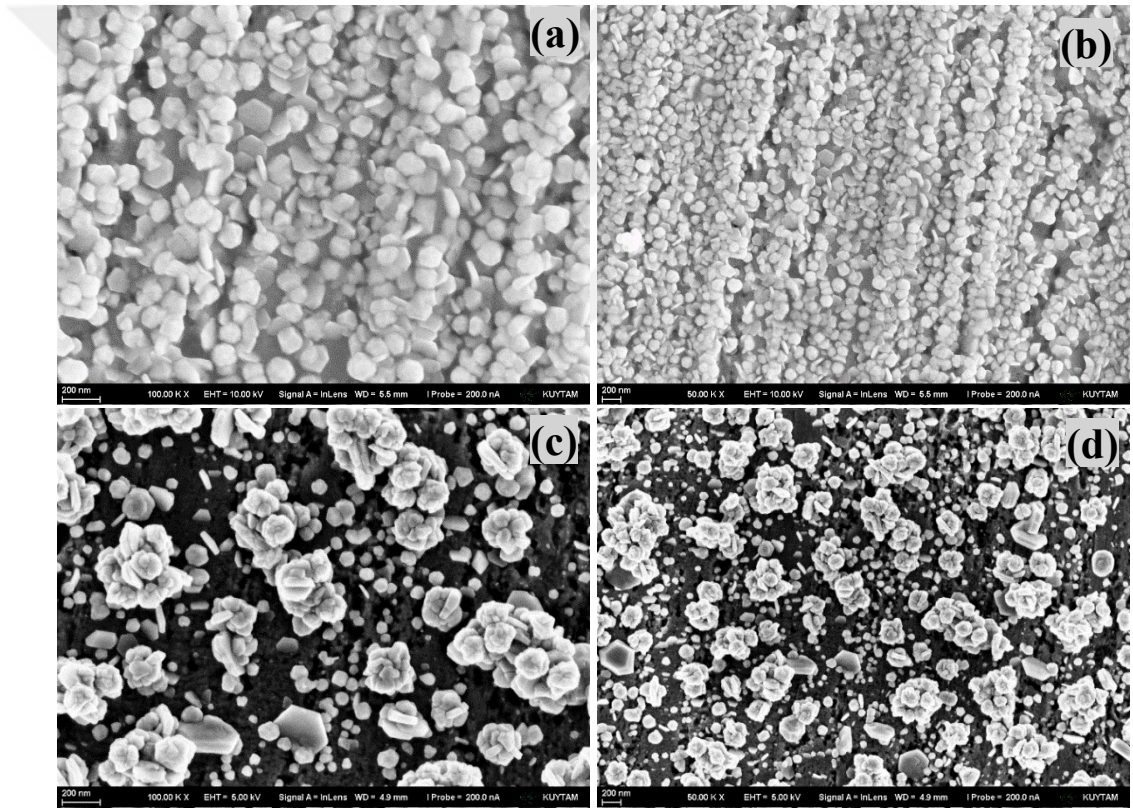

Figure 2-4: SEM image of (a-b) Ag/Cu (c-d) flowerlike-Ag/Cu

The first substrate is a silver deposited sample with a 5-minute reaction time. The second substrate was generated by repeating the 5-minute reaction time three times. By repeating the silver deposition step, flower-shaped Ag nanoparticles were obtained. This shape is favored for a variety of reasons, all of which result in electromagnetic enhancement. The combination of aggregated nanostructures and roughened metal surfaces results in anisotropy, which in turn can give rise to a robust electromagnetic coupling [50]–[52]. Flower-shaped particles have been built up of assembled Ag nanoparticles. The

accumulation on top of each other increased the roughness of the substrate. Furthermore, its design assisted in the creation of more sharp edges, resulting in hot spots. Shape has anisotropically distributed Ag NPs and nano-gaps are formed. A large number of active sites were generated both within the particle and between neighboring particles. To summarize, roughness, sharp edges (hot spots), and nanogaps are all desirable qualities for obtaining an ultra-high sensitive SERS substrate.

The surface composition of the copper substrates was examined using X-ray photoelectron spectroscopy (XPS), shown in Figure 2-5. Figure 2-5(a) and (b) belongs to Cu 2p spectra of the Ag/Cu and flowerlike-Ag/Cu respectively. They have two major peaks that corresponded to Cu $2p_{1/2}$ and Cu $2p_{3/2}$ at 932.7 eV and 952.4 eV, accordingly. The peaks at 933.4 and 953.78 eV refer to the Cu species that have been oxidized. Additionally, the satellite peaks lie between 940-945 and 960-965 eV [53]. Ag 3d spectra with binding energies of 368.1 eV and 374.1 eV are displayed in Figure 2-5 (c). Similar intensities between Ag/Cu and flowerlike-Ag/Cu indicate that the Ag composition on the surface is similar to each other.

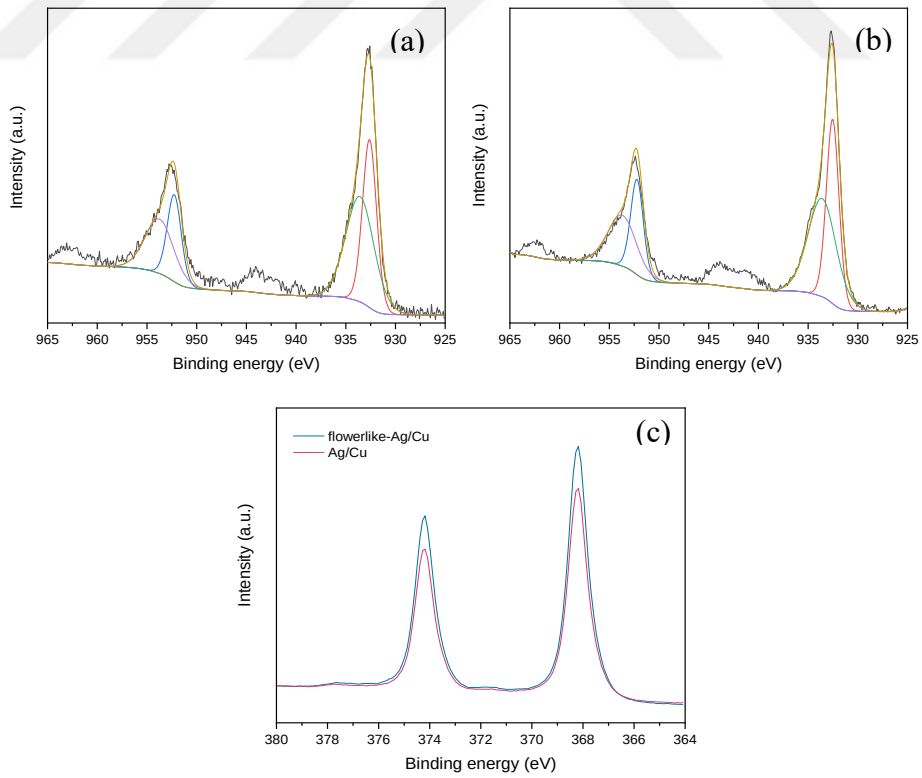

Figure 2-5: XPS spectrum of Cu 2p (a) Ag/Cu (b) flowerlike-Ag/Cu, Ag 3d (c) both substrates

2.3.2 Detection of RhB by SERS using NP modified Cu substrates

Rhodamine B (RhB) was used as a probe molecule in this study to analyze the SERS activity of Ag NPs with various morphologies on Cu plates. RhB has been applied to SERS studies because to its distinctive Raman signals and N-containing molecule structure. Raman spectrum of the of RhB detection performed on the Ag/Cu and flower-like Ag/Cu substrate is shown in Figure 2-6. With SERS enhancement effect, decreased concentrations of RhB ranging from 10^{-4} M to 10^{-8} M could be detected. As predicted signals become weaker as concentration decreases. The Raman spectrum of the RhB displays three major bands located at 1357, 1507, 1646 cm^{-1}. Intensities of these prominent bands are strong and can be detectable at low concentrations. SERS peaks of RhB spectrum are attributed to aromatic stretch vibrations (1646, 1527, 1357 cm^{-1}), C–C bridgeband stretch vibration (1279 cm^{-1}), C–H in-plane bend vibration (1198 cm^{-1}) [54].

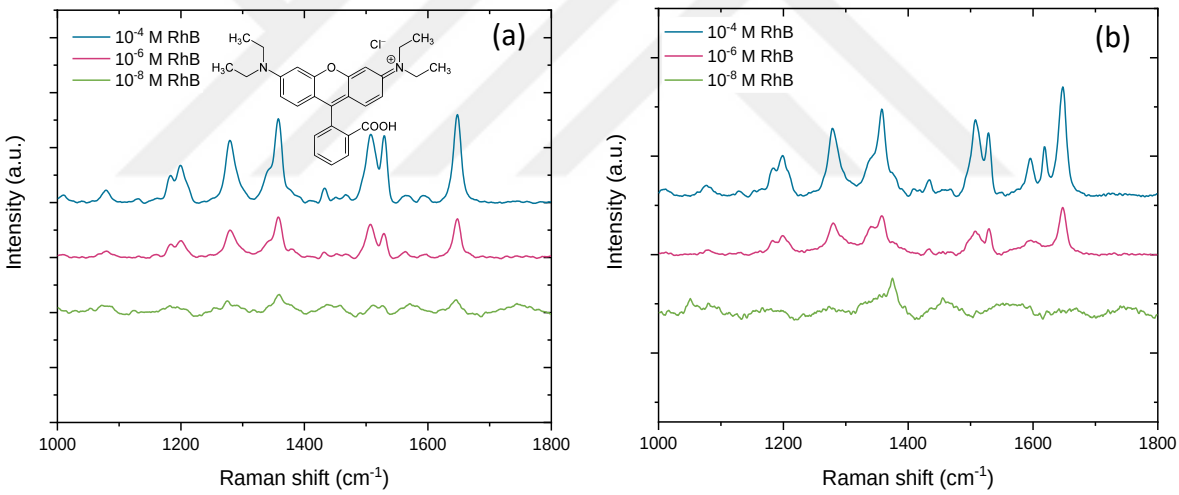

Figure 2-6:SERS spectra of 10^{-4} M to 10^{-8} M RhB detection by (a) Ag/Cu (b) flowerlike-Ag/Cu substrate

Raman spectrum of bare Cu plate is shown in Figure 2-7. Cu does not exhibit any interference peaks between 800 and 1800 cm^{-1}, where probe molecule detection is explored, and it has a featureless background under SERS, as was before mentioned.

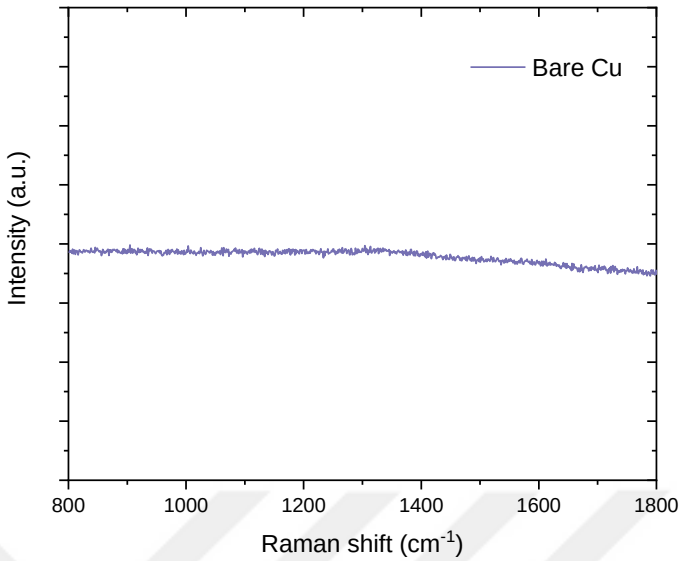

Figure 2-7: Raman spectrum of bare copper plate

2.4 Conclusion

In this chapter, synthesis, characterization, and SERS analysis of silver nanoparticle decorated copper substrates is investigated. Silver nanoparticles were successfully synthesized on the copper plate with a good distribution on the surface. Their presence is validated by SEM and XPS analysis. Substrates that have different morphologies and distributions created by changing the silver salt deposition time and method. To obtain a highly sensitive SERS substrate, the form, size, and interparticle space of the nanoparticles must be considered. SEM pictures aided in deciding on the best possible morphology. XPS results confirmed the surface chemical structure of the prepared substrates. The Cu 2p spectrum validated the presence of distinct oxidation states on the surface, whereas the Ag 3d spectrum supported the presence of elemental form of Ag nanoparticles (Ag^0), and the strength of peaks demonstrated the similar composition of Ag produced on both substrates.

SERS study performed with the probe RhB molecule between 10^{-4} M to 10^{-8} M. The primary peaks of RhB at 1357, 1507, and 1646 cm^{-1} correspond to different vibrational modes of the molecule could be observed. The detection limit of 10^{-8} M was achieved using the flowerlike Ag/Cu substrate.

Chapter 3:
SERS SUBSTRATE: SILVER AND GOLD NANOPARTICLES DECORATED COPPER

3.1 Introduction

Silver is well-known as a good electromagnetic enhancer. In comparison, gold has greater stability than silver, but its enhancing factors are often smaller. However, because silver is quickly oxidized, its enhancement will decrease over time. Developing a substrate for SERS that uses both silver and gold will enable the exploitation of each material's beneficial characteristics [55]. The SERS enhancement factor is greater when Au and Ag are combined.

As mentioned before, the shape of the nanoparticles plays an important role in the development of the substrate. Hu et al. investigated the SERS performance of gold nanorods utilizing cationic and anionic dye molecules. They stated, gold nanorods demonstrates better SERS performance compared to gold nanospheres because of the anisotropy. They exhibit excellent chemical durability, configurable plasmon absorption bands and strongly curved surface characteristics with higher local field enhancement [56].

Tong et al. developed a SERS substrate for detection of hexamethylenetetramine and employed Au and Ag together on the substrate. They claimed that the wider and stronger plasmon resonance of the combined nanoparticles led to a larger enhancement on Raman signals than using only gold [57]. Küstner et al. worked with gold/silver nanoshells for SERS in bioanalytical applications, reporting a 180-fold increase in peak intensity for the combination of gold and silver nanoshells compared to single gold particles [58]. As a result of the high enhancement factors, it is well known that the synergistic effect of gold and silver together will allow going lower limit of detections.

In Chapters 2 and 3, RhB was used as a probe molecule to investigate the performance of the SERS substrate. The addition of gold enabled the detection of the RhB molecule at concentrations as low as 10^{-16} M. Thus, depending on this advancement, target molecule; nitrite detection is being studied.

Griess test is a standard method for nitrite monitoring. Griess reagent and nitrite solution undergo a reaction, and a red-pink color is generated. The presence of nitrite is

indicated by this color. However, at low concentrations, color change is not visible, and the approach has a limited sensitivity. The molecular spectral fingerprints of analytes can be identified by SERS devices and the sensing signal can be acquired by directly obtaining the analyte's SERS spectrum [1].

Nitrite detection is not achievable utilizing the nitrite molecule directly, hence SERRS (Surface-Enhanced Resonance Raman Scattering) is used to make it possible. The SERRS effect can be used to improve SERS signals even further. Peaks are enhanced when the analyzed molecule's absorption matches the frequency of the incident laser of the Raman spectrometer. This resonance effect enables single-molecule detection[59], [60]. An effective method for the indirect detection of nitrite is the use of azo dyes as active Raman molecular probes. A coupling reaction occurs between phenol and diazonium ions, producing azo dyes[61].

Li et al. reported nitrite detection on SERS substrate based on modified azo dye formed by 4-aminothiophenol, nitrite, and N-(1-naphthyl) ethylenediamine dihydrochloride in acid conditions. They used both silver and gold nanoparticles and reached 9.0 $nmolL^{-1}$ limit of detection [60]. Zheng et al. studied nitrite detection, used silver nanopyramids and gold nanostars and functionalize the NPs with 1-naphtylamine and 4-aminothiophenol, respectively. They reached a detection limit of 0.6 pg/mL for nitrite in water [1].

3.2 Materials and Methods

3.2.1 Materials

All the chemicals were used as received without further purification. Polycrystalline Cu foil (25 μm thick, > 99.99%, MTI corporation), silver nitrate ($AgNO_3$, Sigma-Aldrich), auric acid ($H[AuCl_4]$, Sigma-Aldrich), ethylene diamine tetraacetic acid (EDTA), stannous chloride ($SnCl_2$, Sigma-Aldrich), hydrochloric acid (HCl, 37%, Sigma-Aldrich), 4-Aminothiophenol (4-ATP, Sigma-Aldrich), naphthylamine (1-NA, Sigma-Aldrich), Rhodamine B (RhB, Alfa Aesar), sodium nitrite ($NaNO_2$. Sigma-Aldrich). All solutions are prepared with distilled water.

3.2.2 Synthesis of Ag- Au modified Cu substrates

Synthesis of Ag modified copper substrates used in this chapter were explained in Section 2.2.2. Formerly prepared Ag-copper substrates (Ag/Cu and flowerlike-Ag/Cu) further immersed into 5 mL of $SnCl_2$ solution (1.5mM) for 10 minutes, rinsed with water. Later immersed in mixture of 3 mL of $H[AuCl_4]$ (3 mM) and 5 mL of EDTA (3 mM) for 2 minutes, to obtain gold nanoparticles on top of silver nanoparticles. Finally, to avoid the over exposure to the gold solution and stopping the reaction, it is crucial to promptly dry the substrate using nitrogen gas to eliminate any residual droplets on the surface.

3.2.3 Synthesis of Azo dye

4-ATP was dissolved in 0.01 M HCl, and 1 mM solution was obtained. 1mM 1-NA solution was prepared by dissolving in deionized water. Varying nitrite concentrations ($1x10^{-4}$ M to $1x10^{-14}$ M) were prepared by diluting the nitrite stock solution. Then 10 ml nitrite solution and 1mL 4-ATP were mixed to obtain diazotization reaction. The diazonium salt was mixed with 1 mL 1-NA and azo dye formation was observed with color change. Color was turned to orange-pink in higher concentrations of nitrite samples.

3.2.4 Structural characterization of Ag-Au modified Cu substrates

Surface chemical structure of the films were analyzed with X-ray photoelectron spectroscopy (XPS, Thermo K-Alpha) with Al Kα source. The fittings for the experimental data were done with Avantage software. Morphology of the NP deposited films were investigated with Field Emission Scanning Electron Microscopy (FESEM, Zeiss Ultra Plus).

3.2.5 Detection of RhB and Nitrite by SERS using Ag-Au modified Cu substrates

RhB detection was done by the same procedure explained in Section 2.2.5. Raman spectra were recorded using Raman microscope (Renishaw Invia) with 50X objective lens (NA=0.75). A 532 nm laser with a power of 16.3 mW was employed as an excitation source for RhB detection. A 785 nm laser was used as an excitation source for nitrite detection. For each measurement 10 spectra were collected from different spots on the sample to ensure the repeatability. To detect nitrite, the SERS substrates were dipped in

0.5 mL Azo dye solution synthesized with varying nitrite concentrations ($1x10^{-4}$ M to $1x10^{-14}$ M) for 15 minutes and allowed to dry naturally. Subsequent to drying substrates were rinsed with distillate water and dried again.

3.3 Results and Discussion

3.3.1 Structural Characterization of substrates

As mentioned in the Chapter 2, Ag NPs modified Cu substrates were synthesized on the surface of copper plate with using reducing agent; stannous chloride and capping agent; EDTA. SERS performance was investigated and 10^{-8} M of LOD was obtained for RhB probe molecule. In this chapter as depicted in Figure 3-1, Au NPs deposited onto Ag modified substrates to further enhance the SERS behavior. Two types of substrates obtained: Ag-Au/Cu substrate and flowerlike-Ag-Au/Cu substrate.

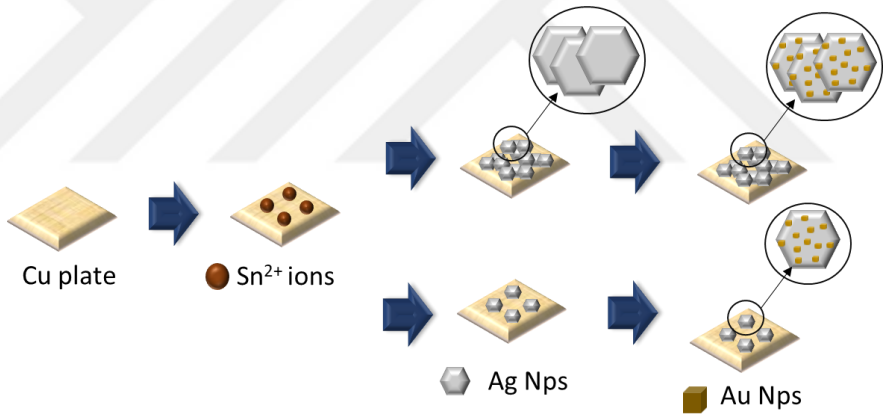

Figure 3-1: The synthesis of flowerlike-Ag-Au/Cu and flowerlike- Ag-Au/Cu SERS substrate is shown schematically.

Cubic gold nanoparticles were obtained from the procedure of 2 minutes of deposition of metal salt and the capping agent. According to the literature, EDTA can act as a reducing and capping agent [46]. Shape control of nanoparticles is dependent on particle growth kinetics and surface energies of different facets. However, due to the faceting tendency of the stabilizing agent, different types of stabilizing agents used in the synthesis result in different shapes of nanoparticles. The surface energy order of the FCC crystal structure is given in the equation; $\gamma\{111\} < \gamma\{100\} < \gamma\{110\}$. M. Kim et al. and Sau and Murphy investigated the cubic structure of gold nanoparticles using cetyltrimethylammonium bromide (CTAB) as a stabilizing agent and concluded that

binding preference on facets of CTAB resulted in the cubic shape of Au nanoparticle. They stated CTAB has a tendency for binding to the {100} faces rather than the {111} faces, allowing Au ions to be deposited on the {111} faces which cause them to vanish and {100} faces to form. [62], [63]. Merging literature with our case, EDTA might be considered to support the formation of the cubic form of the particles obtained in this study.

As shown in Figure 3-2 a SERS substrate containing gold particles without the addition of silver was constructed to evaluate the SERS enhancement of gold nanoparticles on Cu plate. The homogeneous dispersion of gold nanoparticles on the copper plate is demonstrated by SEM pictures. Higher immersion time results in denser Au nanoparticle distribution. SERS data for gold-deposited samples were obtained. SERS enhancement of the substrate was expected to be limited because gold has lower enhancement factors.

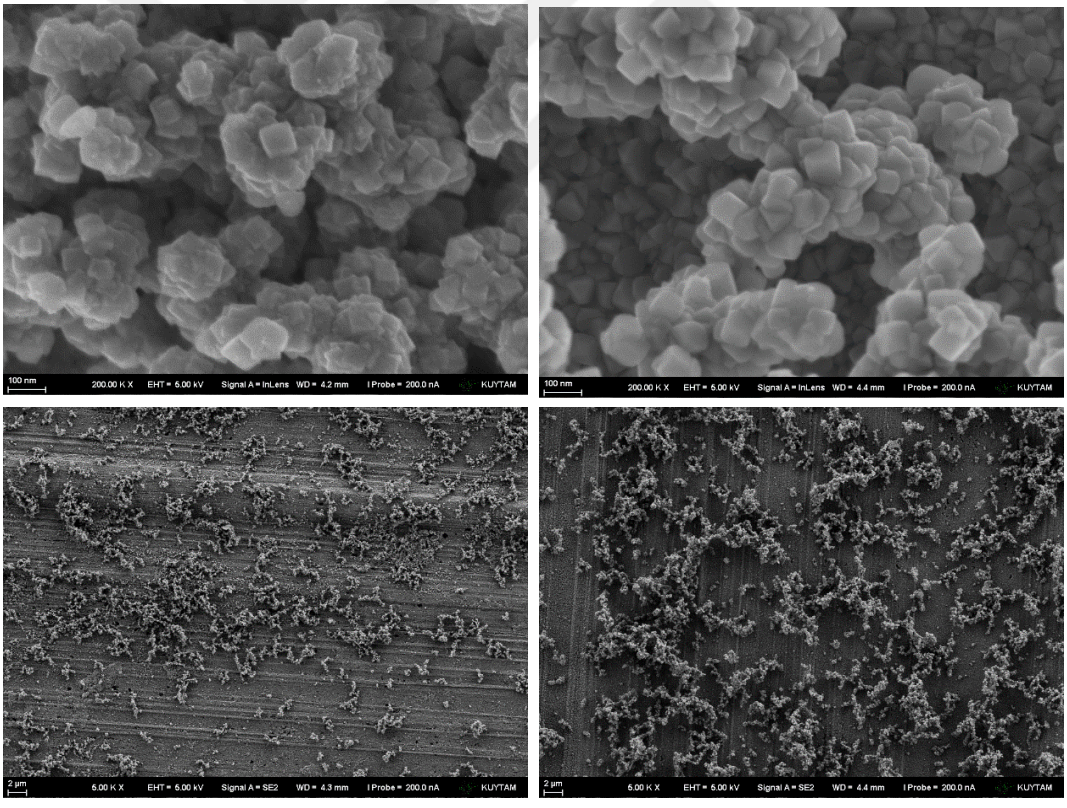

Figure 3-2: SEM image of Au deposited Cu substrates; (left)10 minutes, (right) 20 minutes.

From the sorts of substrates discussed above, the first type (Au-Ag/Cu) is illustrated in Figure 3-3. It is produced by treating the Ag/Cu substrate mentioned in Chapter 2 with

gold. At greater magnifications(500kx), cubic gold nanoparticles can be seen well established above silver nanoparticles. The SEM image of second type of substrate shown in Figure 3-4, was created by treating a flowerlike-Ag/Cu substrate with gold. Despite the Ag-Au/Cu substrate, it has a rougher surface, which causes hot spots due to sharp edges and curvatures caused by the flower-shaped deposition process. According to SEM pictures, gold nanoparticles were distributed equally on both substrates.

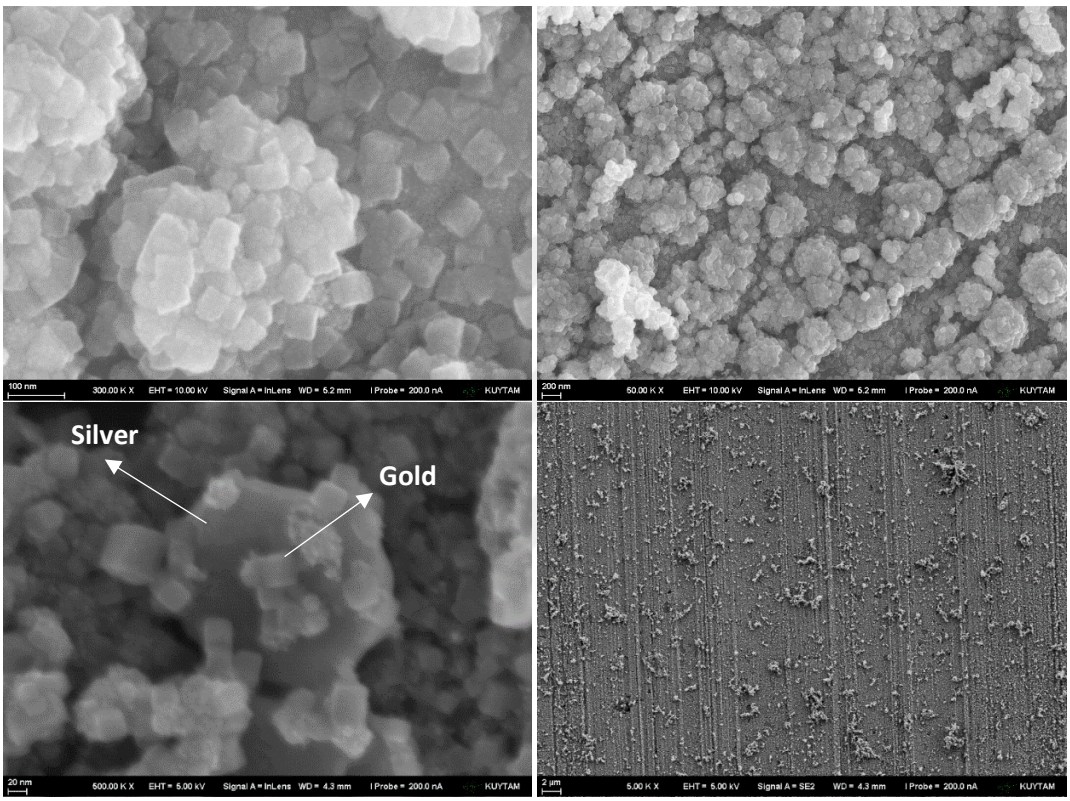

Figure 3-3: SEM images of Au-Ag/Cu substrate

As seen from Figure 3-5, longer reaction time for both substrates were studied. Figure 3-5(a) demonstrates SEM image of Ag-Au/Cu substrate. Figure 3-5(b) demonstrates flowerlike-Ag-Au/Cu substrate with 4 minutes gold nanoparticle reaction time. Gold nanoparticles begin to over-populate on the surface as reaction time increases, inhibiting the active sites of silver nanoparticles by covering them. This also made it difficult for analyte molecules to connect to the silver site of the substrate. Moreover, hotspots caused by nanogaps are hindered by excessive growth of the particles.

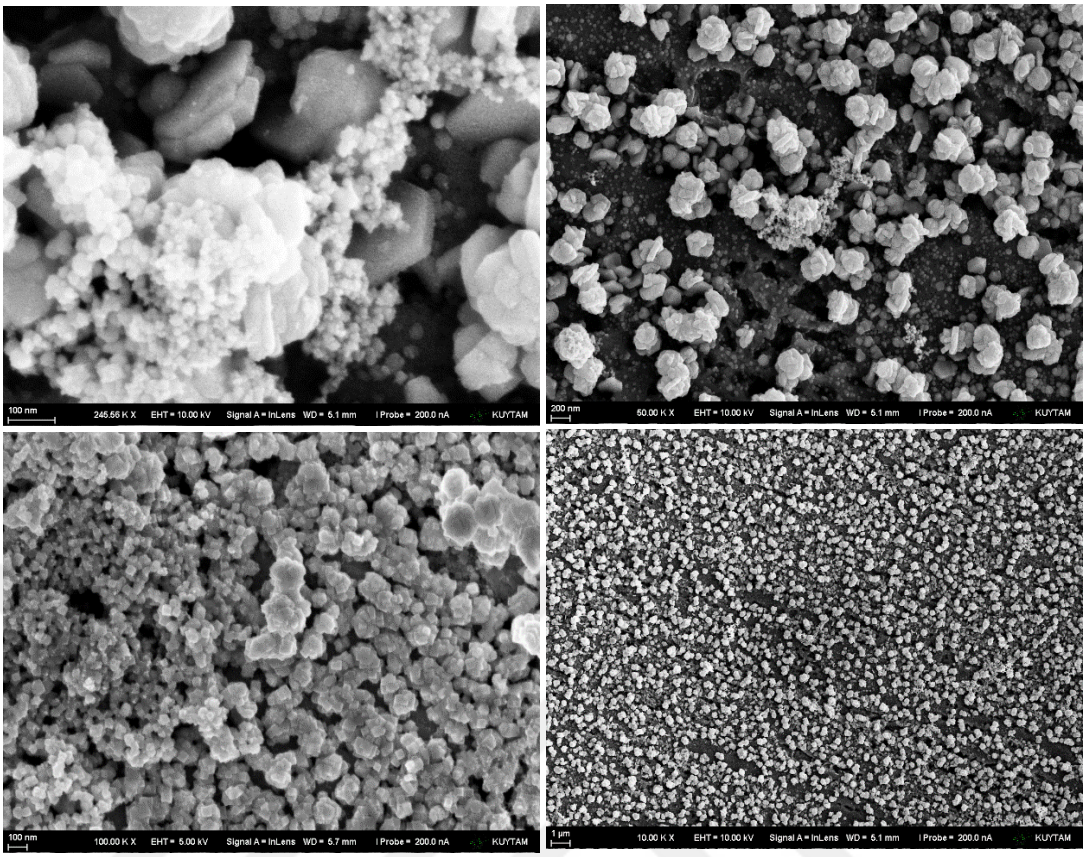

Figure 3-4:SEM image of flowerlike-Ag-Au/Cu substrate

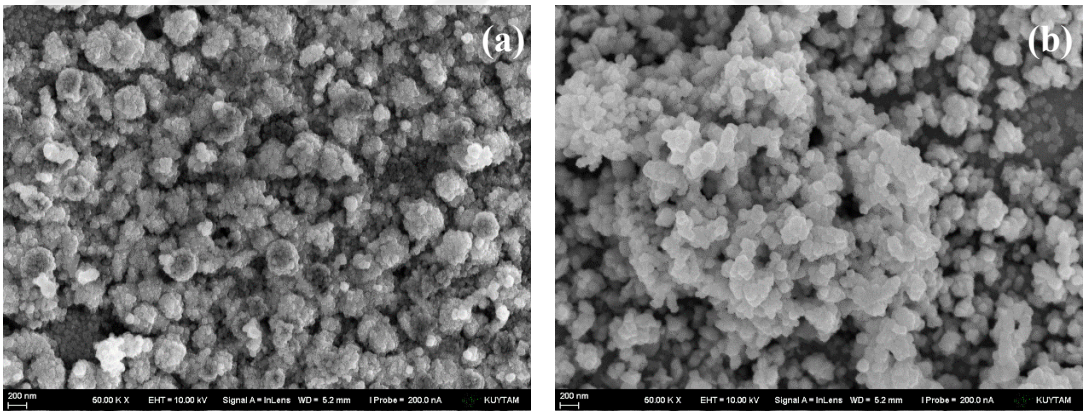

Figure 3-5: SEM image of 4 minutes reaction time of gold deposition samples (a) Ag-Au/Cu substrate and (b) flowerlike-Ag-Au/Cu substrate

To evaluate the surface structure XPS data obtained and demonstrated in Figure 3-6. Figure 3-6(a) belongs to the Au 4f and has two peaks at the binding energies at 84.0 and 87.7 eV. Peaks belongs to the $Au4f_{7/2}$ and $Au4f_{5/2}$ spin−orbit coupling, associated with elemental gold (Au^0) [64]. Ag-Au/Cu and flowerlike-Ag-Au/Cu substrates showed the same intensity peaks of Au-4f, indicating a similar distribution of Au nanoparticles on the surface after 2 minutes of deposition. Figure 3-6(b) belongs to the Ag 3d spectrum and

has two peaks at the binding energies at 368.1 eV and 374.1 eV. Peaks corresponds to the Ag $3d_{3/2}$ and Ag $3d_{5/2}$ respectively, which is related to elemental silver (Ag^0) [31].

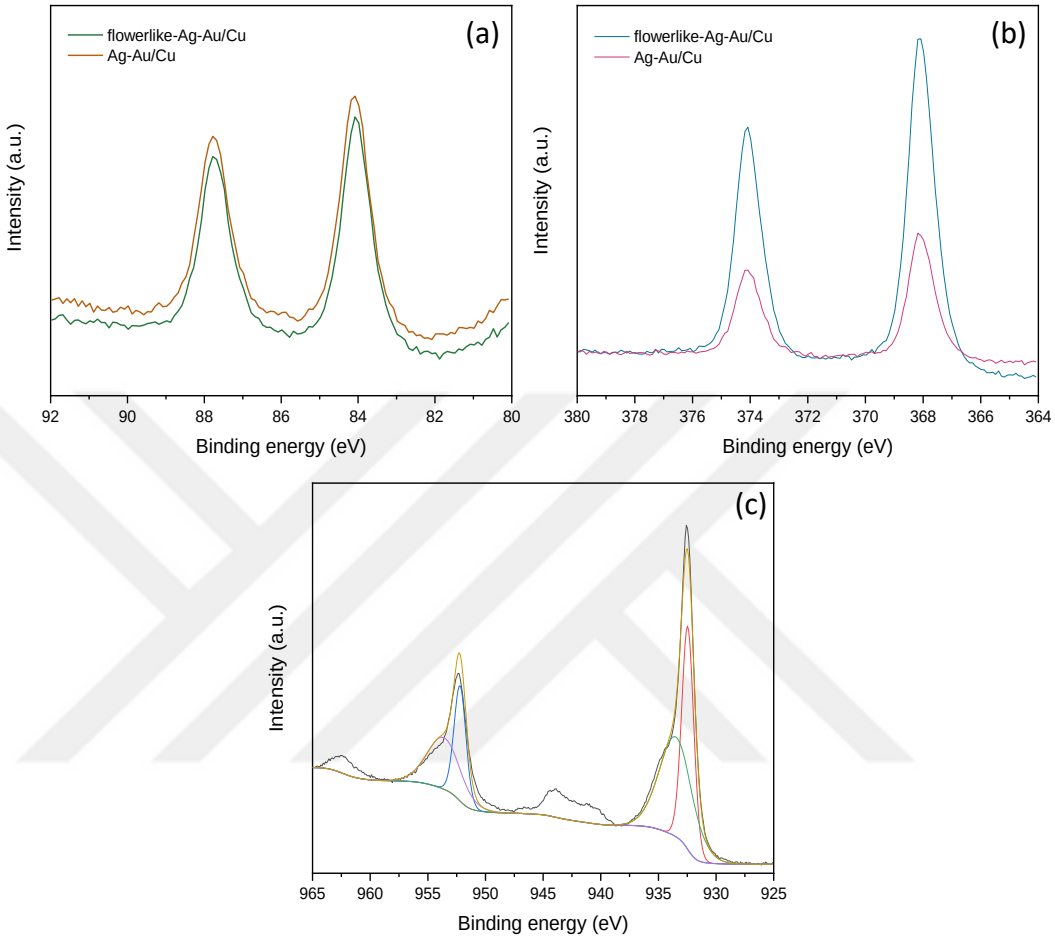

Figure 3-6: XPS spectrum of Au 4f (a)both substrates, Ag 3d (b) both substrates, Cu 2p (c) Ag-Au/Cu

The flowerlike-Ag-Au/Cu has higher intensity peaks than the Ag-Au/Cu. Before Au deposition, both substrates revealed equal intensity of Ag peaks in the XPS study, as shown in Chapter 2 Figure 2-5 (c). While the surface of the Ag-Au/Cu substrate has a larger coverage of Au NPs, the surface of the flowerlike-Ag-Au/Cu substrate has both gold and silver NPs, which may explain the higher SERS performance of the flowerlike-Ag-Au/Cu substrate. To learn more about the composition of the surface, Cu composition characterized by the XPS. Figure 3-6(c) shows XPS spectra of Cu 2p. It displayed two main peaks at the 932.7 eV and 952.4 eV, matching Cu $2p_{1/2}$ and Cu $2p_{3/2}$. The oxidized Cu species are represented by the peaks at 933.4 and 953.78 eV. Furthermore, the satellite peaks are positioned between 940-945 and 960-965 eV [53]. According to XPS analysis,

the gold to silver ratio on Ag-Au/Cu samples is 1-1, whereas the gold to silver ratio on flowerlike-Ag-Au/Cu samples is 1-3.

3.3.2 Detection of RhB by SERS using Ag-Au modified Cu substrates

The SERS performance of Ag-AuNPs/Cu after Au deposition was found to be superior to that of Ag/Cu substrate. The synergic effect of gold and silver is evaluated in Figure 3-7 by comparing the intensity of peaks formed by the 10^{-6} M RhB probe molecule on different substrates. When the peak at 1646 cm^{-1} was considered, gold addition on the Ag structured substrate resulted in a 7-fold increase in intensity. As mentioned in Section 1.2, gold nanoparticles are known to have lower enhancement factors than silver nanoparticles. When comparing the bimetallic substrate to the Au/Cu substrate, the intensity obtained is found to be 160 times higher.

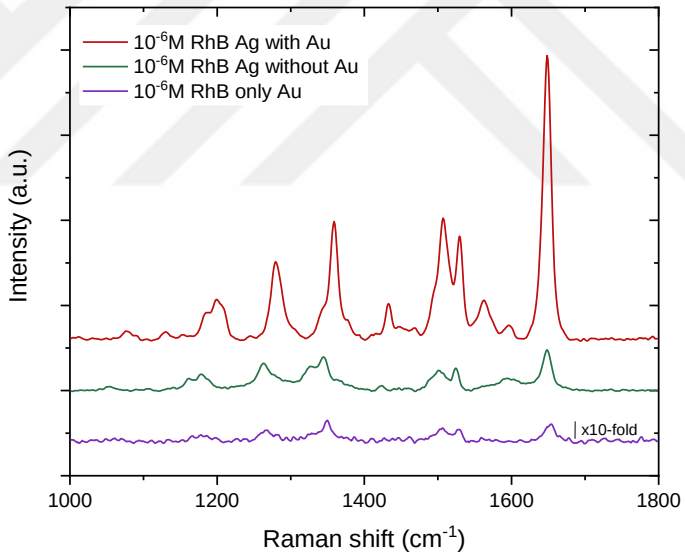

Figure 3-7: Difference between SERS spectra of 10^{-6} M RhB detection by (red) flowerlike-Ag/Cu and (green) flowerlike-Ag-Au/Cu and (purple) Au/Cu substrate

Moreover, with addition of Au nanoparticles the detection limit is dramatically improved to 10^{-16} M. The extreme "hot spots" are generated by plasmonic interaction between the Au and the Ag nanoparticles, greatly enhancing the overall SERS performance [1]. The SERS spectra of RhB adsorbed on Ag-Au/Cu is shown in Figure 3-8. The Figure 3-8 shows characteristic RhB peaks between 1000 and 1800 cm^{-1}, peaks

appeared at 1189, 1279, 1357, 1507, 1646 cm^{-1}. Three major peaks can be detectable at the lowest detection limit are 1357, 1507, 1646 cm^{-1}.

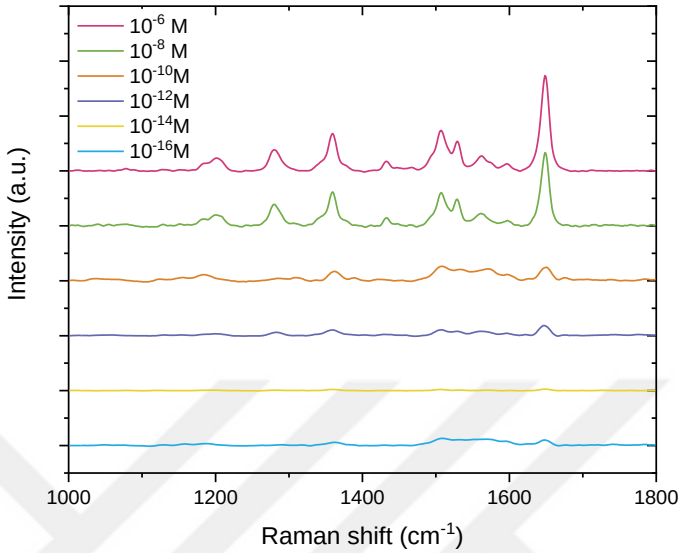

Figure 3-8: SERS spectra of 10^{-6} M to 10^{-16} M RhB detection by Ag-Au/Cu substrate

Figure 3-9 displays the SERS spectra of RhB adsorbed on flowerlike-Ag-Au/Cu. 10^{-4} M to 10^{-16} M detection range of RhB is shown.

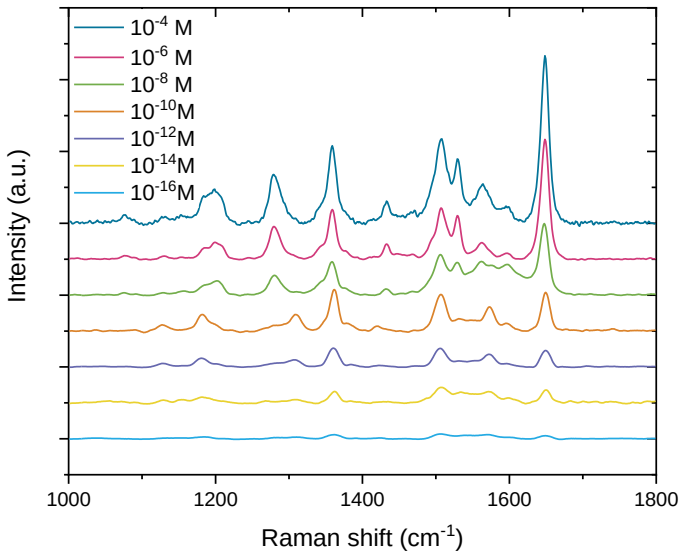

Figure 3-9: SERS spectra of 10^{-4} M to 10^{-16} M RhB detection by flowerlike-Ag-Au/Cu substrate

Flowerlike-Ag-Au/Cu substrate demonstrated higher intensity peaks than the Ag-Au/Cu substrate, attributed to the differences in morphology of both substrates. Aggregated nanostructures, roughened metal surfaces, anisotropy can lead to strong electromagnetic coupling [50]–[52].

These findings suggested that AgNP shapes did, in fact, play a significant role in boosting target molecules' SERS signals. Therefore, we select the Ag-Au/Cu substrate in the shape of a flower as the subject of our ongoing nitrite detection research.

SERS spectra of 10^{-4} M RhB were measured at 10 locations to illustrate the repeatability of the SERS signal of flower-shaped Ag-AuNPs/Cu shown in Figure 3-10. The goal was to determine if the flower-shaped Ag-AuNPs/Cu substrate provided robust SERS enhancements for RhB molecules at the specified concentration. The results demonstrated that the SERS signal intensities at all ten locations were remarkably consistent, with minimal variation observed in the Raman peaks.

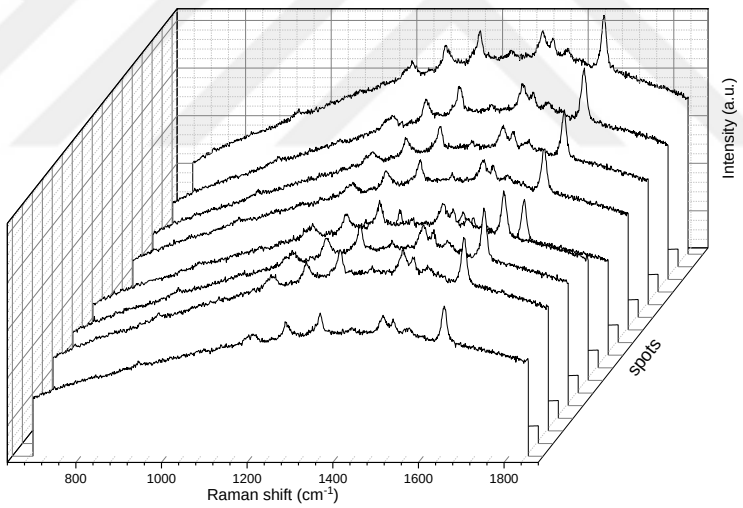

Figure 3-10: SERS spectra of 10-4 M RhB with flowerlike-Ag-Au/Cu substrate from 10 locations.

3.3.3 Detection of Nitrite by SERS using Ag-Au modified Cu substrates

Due to the limited chemical and physical absorbability's of metal surfaces, the SERS of nitrite is weak [60]. The diazo reaction of amino groups and nitrite ions, followed by the azo reaction, has been developed to facilitate SERS detection of nitrite ions in acid environments. As seen in Figure 3-11 ,the diazotization reaction between the coupling agent,1-naphthylamine (1-NA) and the aromatic amine, 4-aminothiophenol (4-ATP) occurs when nitrite ions are present in the assay, resulting in an azo compound that displayed the SERS fingerprints. Under acidic conditions (pH=2-3), nitrite ions react with the amine group of 4-ATP to create diazonium salt. After the diazotization reaction, 1-NA and diazonium salt further react, producing azo dye. Azo dye displays an orange-pink color, indicating that the reaction was formed successfully. When azo dye is deposited on the surface of a substrate, 1-naphtylamine binds the silver NPs from the amine group and 4-aminothiophenol attaches the gold NPs from the thiol group [1], [42], [65].

Figure 3-11:Reaction between 4-ATP, 1-NA and Nitrite molecules forming azo dye compound.

Figure 3-12 shows characteristic peaks of the 4-ATP are clearly spotted where positioned at 1075 cm^{-1}, 1170 cm^{-1}, 1584 cm^{-1}. This peaks are belong to the a_1 type vibrational mode; C-C stretching, C-S stretching, C-H in-plane bending, parallel C-C vibration stretching [66]. 1-NA showed 2 dominant peaks at 1365 cm^{-1} and 1532 cm^{-1}. Three distinct SERS peaks at 1140 cm^{-1}, 1380 cm^{-1}, and 1434 cm^{-1} were produced by the existence of nitrite. The 1140 cm^{-1} peak is attributed to C-N=N vibration with phenyl rings, the 1380 cm^{-1} peak is associated with the C-C vibration with phenyl rings coupled with N=N stretch, the 1434 cm^{-1} peak is assigned to trans isomer of N=N peak [60].

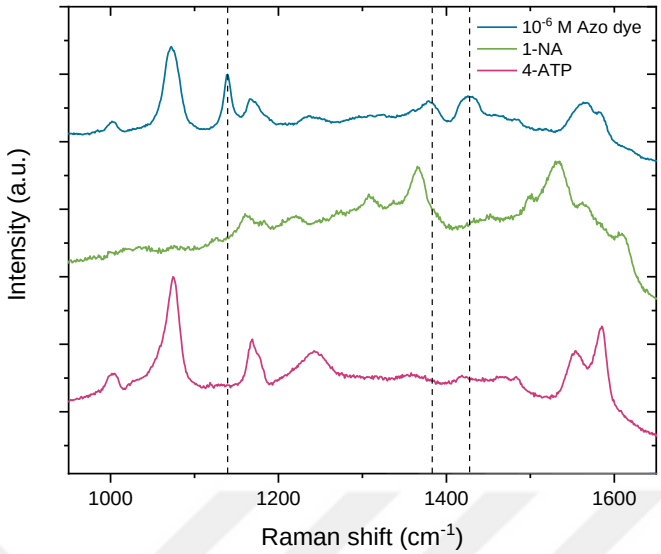

Figure 3-12: SERS spectra of 10^{-6} M Azo dye, 1-NA and 4-ATP on flowerlike-Ag-Au/Cu

From Figure 3-13, it is observed that SERS peaks of nitrite appeared as predicted and the 1140 cm^{-1} peak responded most sensitively to nitrite. It exhibits a well-decreasing tendency from high to low concentration, starting from 10^{-6} M. The limit of detection could measure as low as 10^{-14} M of nitrite concentration used initially before azo dye synthesis.

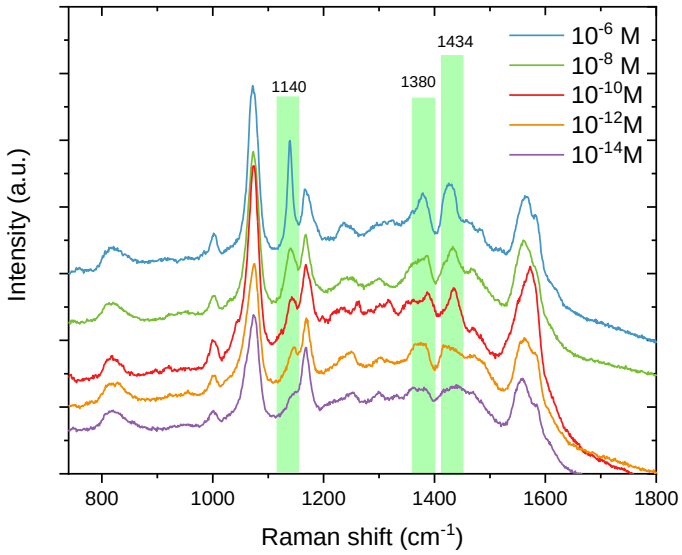

Figure 3-13: SERS spectra of 10^{-6} to 10^{-14}M nitrite detection by flowerlike-Ag-Au/Cu substrate

3.4 Conclusion

This section covers Au nanoparticle deposition to the Ag/Cu and flowerlike Ag/Cu substrates produced in Chapter 2. Gold nanoparticles were synthesized on the copper plate with the same method employed in the Ag nanoparticle synthesis. Synergistic effect of both plasmonic particles utilized to obtain a stable substrate with high enhancement factors. Different reaction times was studied to obtain a uniform distribution of nanoparticles on the substrate without losing active sites of the Ag NPs and nano scale gaps that supports the electromagnetic enhancement with creating hotspots. SEM analysis assisted in the investigation of surface structures. According to the XPS data, the elemental form of Au nanoparticles presents with a similar intensity on both substrates.

SERS performances of gold deposited substrates were investigated via Raman Microscope. For probe molecule detection (RhB), both substrates demonstrated LOD of 10^{-16}M. However, the flowerlike Ag-Au/Cu substrate demonstrated stronger intensity peaks at the lower limit of detection, leading to its selection for nitrite detection. Nitrite detection was studied with accounting on the SERRS method by utilizing azo dye molecule synthesized with diazo reaction for in-direct detection. LOD could reach low as 10^{-14} M.

Chapter 4:

SERS SUBSTRATE: SILVER MODIFIED GRAPHENE AEROGEL FOR RHODAMINE B DETECTION

4.1 Introduction

As mentioned before SERS has two enhancement mechanisms: electromagnetic enhancement (EM), chemical enhancement (CM). In comparison, the CM effect is less powerful than the EM effect; although EM may improve the Raman signal by 5-10 orders of magnitude, CM can improve it by just 2 orders of magnitude. [67]. However, the SERS signals will significantly improve when EM and CM are coupled. Chemical enhancement is a result of physico-chemical interaction of molecule with the substrate. Then the vibrational modes of the Raman cross-sections changes by the change of a molecule's polarizability [68]. Between the molecules of the probe and the substrate, charge is transferred, producing CM [69].

Due to its strong reactivity and abundance of functional groups containing oxygen on the surface and edges, graphene oxide (GO) can be considered one of the most significant derivative of graphene [31]. Through p-p stacking, hydrophobic and electrostatic interactions with polyaromatic regions, and functional groups, GO structures can connect with a wide range of organic compounds [7]. These properties make graphene oxide as a good candidate for the SERS applications. Aside from the 2D graphene oxide structure, the 3D structure known as aerogel has lightweight, excellent chemical stability, high conductivity, and specific surface area features [70]. Three-dimensional (3D) substrates had a large specific surface area compared to low-dimensional modes, which can improve the contact between the goal molecule and the substrate, increasing the sensitivity of detection [71].

In several sturdies graphene and its derivatives coupled with nanoparticles used as SERS substrates. Lv et al. investigated a few layers of nitrogen doped graphene generated using chemical vapor deposition (CVD) and measured its SERS properties using the RhB probe molecule [69]. Kim et al. examined GO coating on polymer functionalized -Ag nanoparticles using rhodamine 6G as a probe and reported a high stability substrate with good reproducibility. GO contributed to their research by hindering AgNP oxidation and its CM property helped in the enhancement of Raman signals [72]. As a first time Liu et

al. employed 3D graphene structure for SERS applications. For the dye molecules, they obtained a SERS enhancement factor ($3.1x\ 10^4$) and a detection limit (10^{-8} M) [71].

Here 3D graphene aerogel supported Ag nanoparticles are studied as a SERS substrate. Metal salt reduction method employed to obtain the nanoparticles on the 3-D graphene aerogel structure. RhB as a probe molecule utilized to investigate the SERS performances of substrates.

4.2 Materials and Methods

4.2.1 Materials

All of the chemicals were used as received, with no further purification. Graphite (natural, 99.9995%, Alfa Aesar), sodium nitrate ($NaNO_3$, 99%, Alfa Aesar), potassium permanganate ($KMnO_4$, Merck Millipore), hydrogen peroxide (H_2O_2, 30%, Merck Millipore), hydrochloric acid (HCl, 37%, Sigma Aldrich), sulfuric acid (H_2SO_4 ,95-97%, Sigma Aldrich) silver nitrate ($AgNO_3$, Sigma-Aldrich), Filter papers (cellulose nitrate, 0.45 μm, Sartorius Stedim Biolab).

4.2.2 Synthesis of Graphene oxide

The modified Hummers method was used to synthesize the graphene oxide. First, a concentrated H_2SO_4 solution was used to dissolve two grams each of $NaNO_3$ and graphite. By placing the reaction vessel in an ice bath, the temperature of the mixture was kept below 5 °C as 12 g of $KMnO_4$ were slowly added to the mixture. Once the $KMnO_4$ had been added, the ice treatment was stopped, and the solution's temperature was allowed to rise to 40°C. After heating the mixture for 30 minutes at 75 °C, the reaction was then stopped by adding 300 mL of ice-cold distillate water and 30% H_2O_2, until yellow foam vanished. The obtained powder washed by using 5% HCl and water, three times each. Graphite oxide solution was sonicated in an ultrasonic bath for 4 hours to exfoliate the solution to produce a single layer nanosheets. Later solution was centrifuged at 1000 rpm for 30 min to discard the aggregated sheets.

4.2.3 Synthesis of Ag modified GA substrate

Figure 4-1 depicts the synthesis of Ag-modified GA substrate. Already synthesized graphene oxide and silver salt mixed in different weight ratios of 0.25 and 0.50 for 30 minutes. Final GO concentration was used as 3.0 g/L at the total volume of 40 mL. The mixture put in PTFE lined stainless-steel bomb and hydrothermal treatment was applied at 180^{o}C for 3 hours. After cooling down naturally, produced monolithic hydrogels immersed in DIW. Solvent-exchange was applied using acetone for 3 times for 3 days. To obtain the aerogel without losing the porous structure, alcogels dried with CO_2 supercritical drying method (Spe-ed SFE-15,000, Applied Separations, Inc.) at 120 bar 50^{o}C for 2 hours.

To reduce the metal salt and obtain the Ag nanoparticles, thermal treatment applied at split tube gas furnace. Powder degassed with Ar at 110^{o}C for 30 minutes The gas was changed to an H_2/Ar combination (10:90, 200 mL per minute), and the temperature was raised to 650 °C with a 5 °C per minute rise. The furnace was maintained at 400 °C for 1 hour. Later, it was cooled down naturally. Obtained powders named as GA/$Ag_{(0.25)}$ and GA/$Ag_{(0.50)}$.

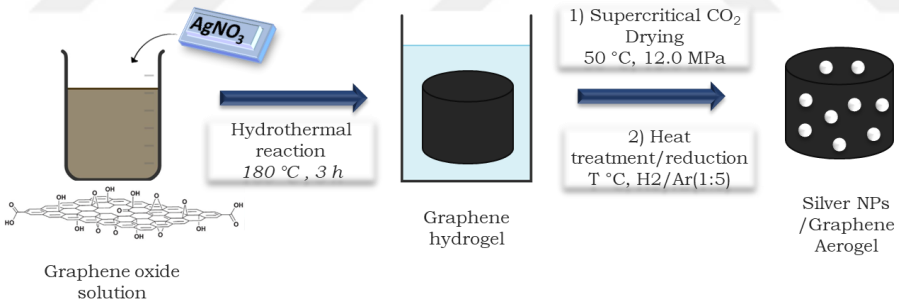

Figure 4-1: Synthesis of Ag-modified graphene aerogel from graphene oxide solution

4.2.4 Structural characterization of Ag-Au modified Cu substrates

Surface chemical structure of the films were analyzed with X-ray photoelectron spectroscopy (XPS, Thermo K-Alpha) with Al Kα source. The fittings for the experimental data were done with Avantage software. Morphology of the NP deposited films were investigated with Field Emission Scanning Electron Microscopy (FESEM, Zeiss Ultra Plus).

4.2.5 Detection of RhB by SERS using Ag modified GA substrate

The RhB solutions were prepared in ethanol in concentrations between 10^{-4}M to 10^{-6}M. Powder substrates were dispersed in ethanol at concentration of 10 mg/mL. Later, for 6 hours, 0.2 mL substrate and 0.5 mL probe molecule were mixed. 10 µL of mixture was dropped onto clean Al plate and dried naturally. Raman spectra were collected via Raman microscope (Renishaw Invia) with 50X objective lens (NA=0.75) and a laser power of 16.3 mW. For the detection, a 532 nm laser was used as an excitation source.

4.3 Results and Discussion

4.3.1 Structural Characterization of substrates

XPS analysis assists in the evaluation of functional groups on graphene oxide structures. Oxygen-containing functional groups are partially removed during the reduction process. The XPS C1s spectrums of $GA/Ag_{(0.25)}$ and $GA/Ag_{(0.50)}$ are shown in Figure 4-2(a) and Figure 4-2(b), respectively. XPS data was deconvoluted into three peaks. Peak at 284.5 eV belongs to the carbon-carbon binding such as C-C/C=C/C-H, 286 eV belongs to the hydroxyl and epoxy groups C-O-C, C-OH, and 289 eV belongs to the carbonyl and carboxyl groups, C=O, O=C-OH [73]. Peaks associated with oxygen functional groups do not exhibit greater intensities because when silver salt is converted into silver nanoparticles, graphene aerogel is also reduced.

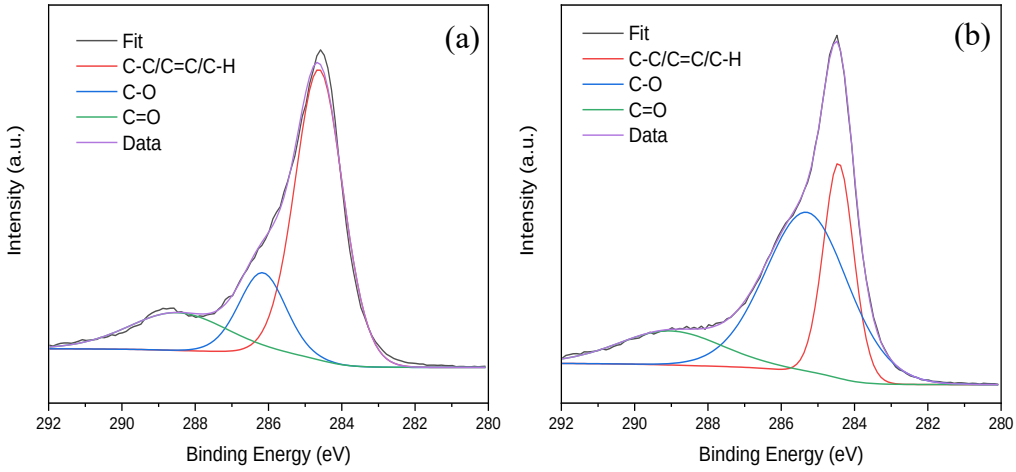

Figure 4-2: XPS C1s spectrum of (a) $GA/Ag_{(0.25)}$ (b) $GA/Ag_{(0.50)}$

Figure 4-3 demonstrates the O1s spectrum, deconvoluted into three peaks. 531 eV, 533.5 eV and 535 eV. Peaks are belonging to the oxygen double bond to aromatic crbon, C=O, oxygen single bonded to aliphatic carbon, C-O-C, oxygen single bonded to aromatic carbon C-OH [74].

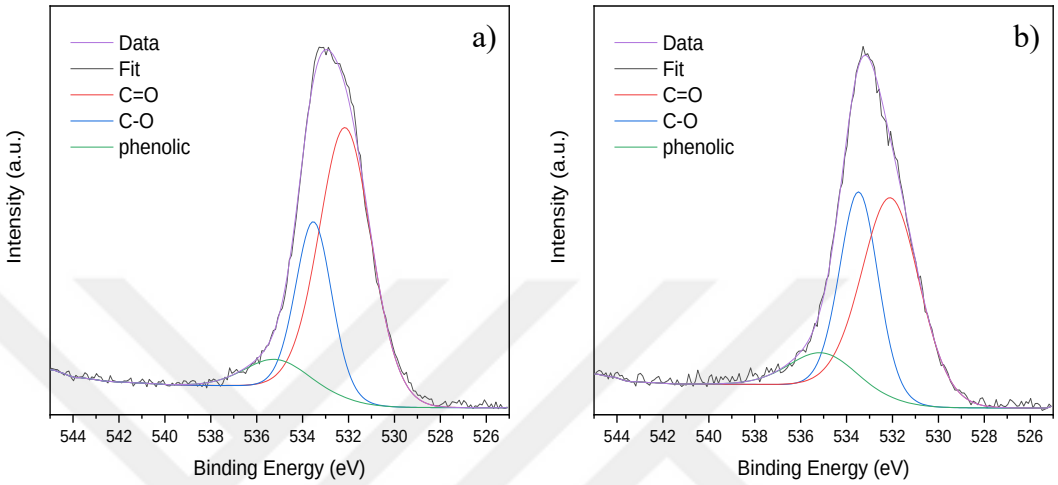

Figure 4-3: XPS O1s spectrum of (a) GA/$Ag_{(0.25)}$ (b) GA/$Ag_{(0.50)}$

Figure 4-4 illustrates the Ag3d spectrum, which has two peaks. 368.1 eV and 374.1 eV corresponds to the Ag $3d_{3/2}$ and Ag $3d_{5/2}$ respectively. The peaks correspond to the metallic Ag presents in the Ag^0 form [31]. Sample with the higher weight ratio of silver (GA/$Ag_{(0.50)}$) displays higher intensity as expected.

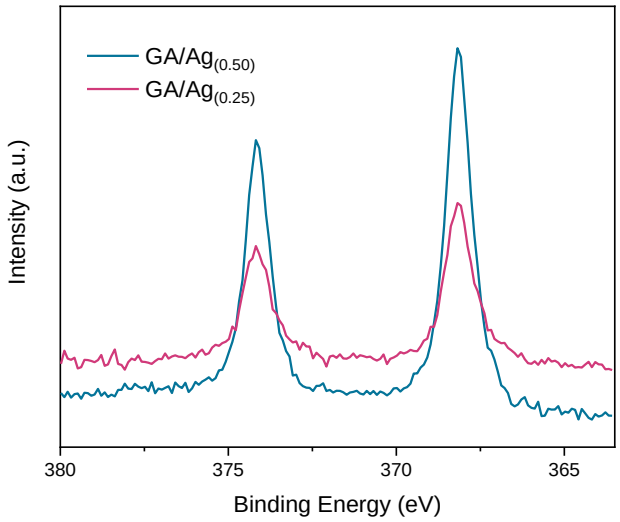

Figure 4-4: XPS Ag 3d spectrum of (a) GA/$Ag_{(0.25)}$ (b) GA/$Ag_{(0.50)}$

The SEM images are shown in Figure 4-5(a) belongs to the non-reduced-GA/$Ag_{(0.25)}$ Figure 4-5(b) belongs to the non-reduced GA/$Ag_{(0.50)}$ (c-d) belongs to the GA/$Ag_{(0.25)}$ X(e-f) belongs to the GA/$Ag_{(0.50)}$.

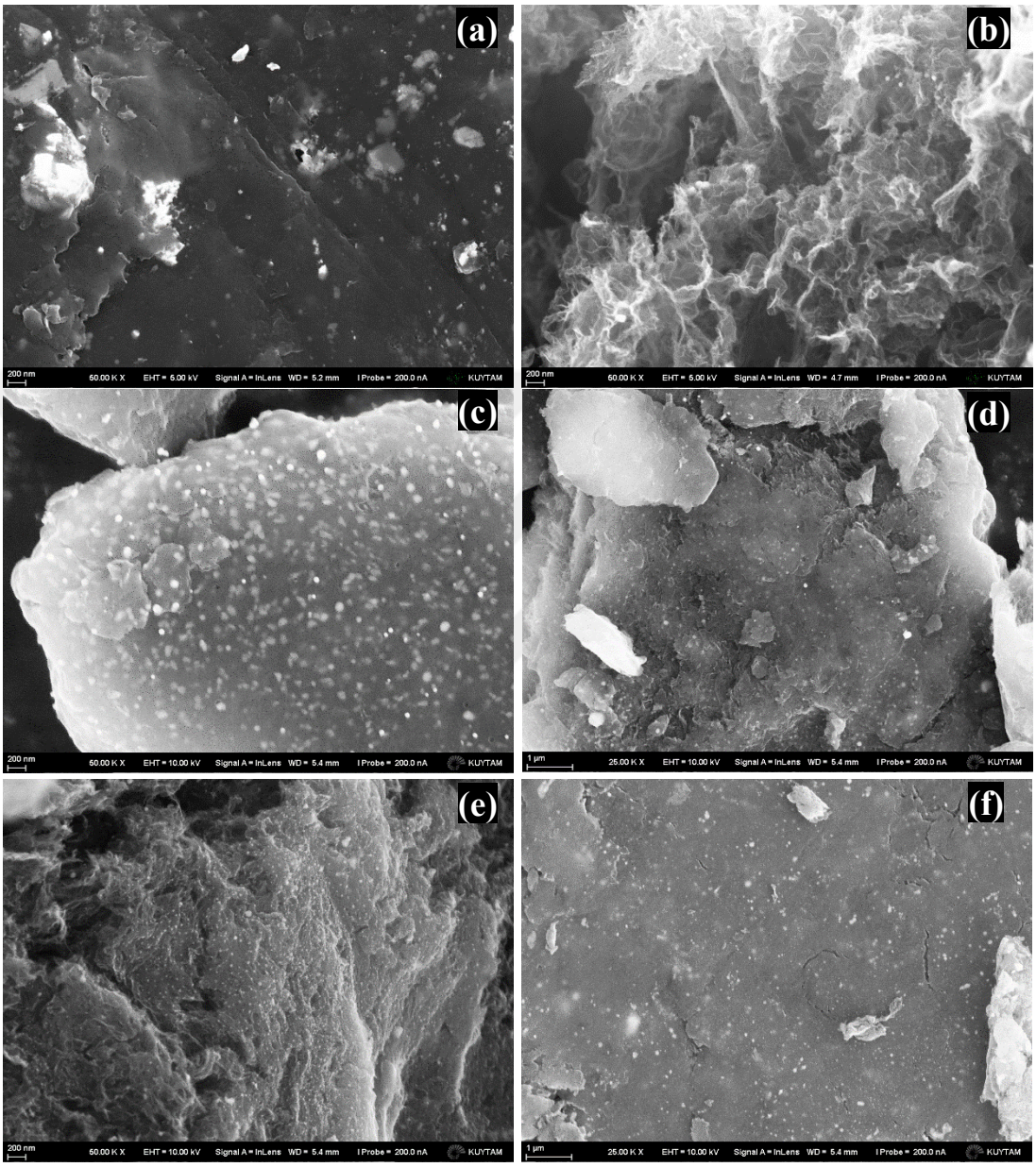

Figure 4-5: SEM image of before reduction; (a) GA/$Ag_{(0.25)}$ (b) GA/$Ag_{(0.50)}$, after reduction; (c-d) GA/$Ag_{(0.25)}$ (e-f) GA/$Ag_{(0.50)}$

Figures show that graphene sheets were layered and joined to create a porous aerogel structure in three dimensions. Figure 4-5(a) and (b) demonstrates, there are few particles visible before reduction, but the most of it is created after reduction. The particles generated from their metal salts prior to reduction could have been caused by the pressure and heat exerted during hydrothermal treatment and supercritical CO_2 drying. SEM

images after reduction process (c,d,e,f,), show GA sheets that have been decorated with aggregated Ag nanoparticles. Because both samples were reduced at the same temperature and time, the nanoparticle sizes are similar. Ag nanoparticles has approximate sizes of 60 nm and has a homogenous distribution on GA.

SEM image of GA/Ag $_{(1)}$ sample has 1 to 1 weigh ratio of GA to Ag shown in Figure 4-6. Because of high Ag nanoparticle density over the GA structure formation of bigger particles and aggregates are observed. The active sites of the Ag atoms were lost as a result of this type of aggregation.

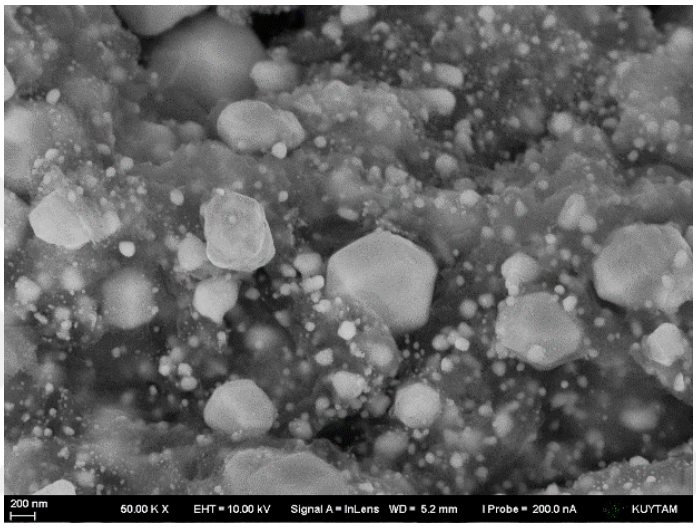

Figure 4-6: SEM image of thermally (400^{o}C) reduced 1.0 wt ratio of GA/Ag.

4.3.2 Detection of RhB by SERS using Ag modified GA substrate

Raman spectra of graphene aerogel is shown in Figure 4-7, displaying 4 different peaks between the 500 cm^{-1} to 3200 cm^{-1}. The bond between the sp^2 carbon group in the ring and the chain elongated, resulting in the formation of the G band. The ring's breathing mode from the aromatic sp2 carbon leads to the formation of the D band. The line shape of the G' band has been generally employed to determine the number of layers present in graphene. The D and D' bands in the Raman spectrum serve as distinctive markers for identifying the edge chirality and various types of defects in graphene, respectively. Additionally, the intensity and frequency of the G and G' peaks provide valuable information regarding the doping levels, strain effects, and isotope concentration in graphene. D and G bands' intensity ratios (I_D/I_G) can be utilized to measure the defect concentration and the types of defects, respectively [16], [71]. In sequence, 1342, 1589, 2682, and 2914 cm^{-1} bands correspond to D, G, D', and G' bands.

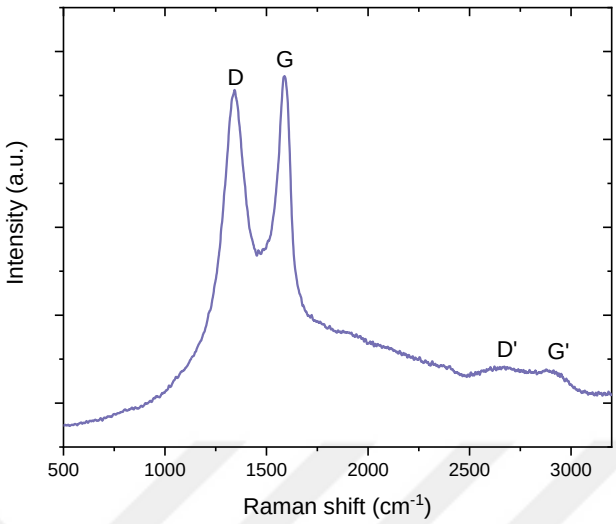

Figure 4-7: Raman spectrum of graphene aerogel

SERS detection of RhB molecule were done by 532 nm laser. As shown in Figure 4-8, RhB characteristic SERS peaks have been identified. The characteristic bands attributed to various RhB vibration modes were detected at 1357, 1507, 1646 cm^{-1}. LOD was found to be 10^{-6} M with the substrate $GA/Ag_{(0.25)}$ and 10^{-5} M with the substrate $GA/Ag_{(0.50)}$. Figure X reveals that the RhB bands are being interfered with by prominent peaks of graphene oxide structure (1342 and 1589 cm^{-1}).

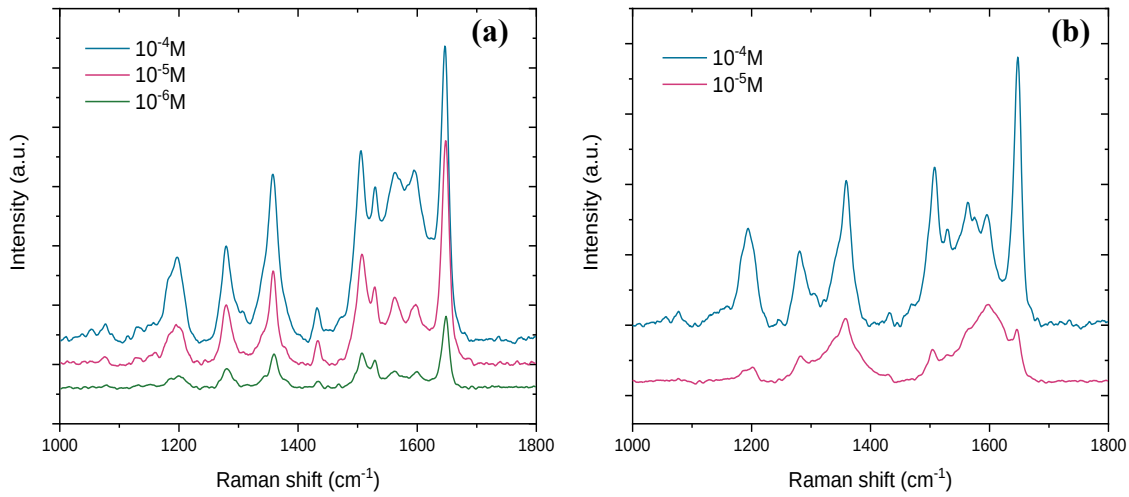

Figure 4-8: SERS spectra of RhB detection by (a) $GA/Ag_{(0.25)}$ (b) $GA/Ag_{(0.50)}$

4.4 Conclusion

In this part silver nanoparticle modified graphene aerogels were synthesized starting from the graphite. Hydrothermal treatment was applied to obtain the 3-D interconnected structure from graphene oxide sheets. Supercritical CO_2 drying was used for producing aerogel structure from the hydrogel form. Different weight ratios of graphene oxide to silver were investigated to find the best composition. Later samples were characterized by SEM and XPS analysis. SEM datas showed homogenous distribution of spherical Ag nanoparticles on the graphene aerogel structure. The existence of oxygen functional groups in graphene oxide, as well as the presence of silver in elemental form, was demonstrated by XPS analysis.

SERS activities of substrates $GA/Ag_{(0.25)}$ and $GA/Ag_{(0.50)}$ were examined using RhB molecules for detection. The LOD was determined to be 10-6 and 10-5, accordingly.

Chapter 5:
CONCLUSIONS & OUTLOOK

In conclusion, this dissertation focused on the development and application of plasmonic metal particle substrates for the detection of nitrogen-derived molecules. The synthesis and characterization of silver (Ag) and gold (Au) nanoparticles on copper (Cu) plates were investigated, along with the production of nanoparticles on a three-dimensional (3D) graphene oxide framework.

The first part of the research involved the synthesis of Ag nanoparticles on Cu plates, second part focused on the effects of Au nanoparticle addition on the already synthesized substrates. Successful assembly of nanoparticles on the Cu plate resulted in a homogeneous distribution of Ag and Au nanoparticles. Various analytical techniques such as scanning electron microscopy (SEM) and X-ray photoelectron spectroscopy (XPS) employed to characterize the surface characteristics and compositions of the substrates.

Third part of the study investigated the production of silver nanoparticles on a 3D graphene oxide framework. Graphene aerogels (GA) with Ag modifications were used as SERS substrates. SEM and XPS analysis confirmed the uniform distribution of Ag nanoparticles on the graphene aerogel structure and showed the surface composition.

The SERS performance of the substrates was evaluated using the probe molecule Rhodamine B (RhB). The flowerlike Ag-Au/Cu substrate exhibited the highest sensitivity, with a detection limit of 10^{-16} M for RhB molecules. Silver modified Cu substrates showed 10^{-8} M, silver modified graphene aerogel substrates showed 10^{-6} M limit of detection. Furthermore, the most promising substrate used for nitrite detection employing the in-direct azo dye method with SERRS detection exhibited 10^{-14} M LOD.

For future works, one promising area for exploration is the gas sensing using the developed substrates. Study can focus on the detection of various nitrogen derived gases. While this dissertation primarily focused on the detection of nitrite, additional investigation into ammonia detection can be employed as an area of research.

Additional investigations could concentrate on environmental monitoring using water or soil samples or disease identification utilizing saliva or breath samples to serve the main objective of this study. To sum up, more investigation and optimization of these substrates could lead to advancements in pollution monitoring and disease diagnosis.

BIBLIOGRAPHY

[1] P. Zheng *et al.*, “Detection of nitrite with a surface-enhanced Raman scattering sensor based on silver nanopyramid array,” *Anal. Chim. Acta*, vol. 1040, pp. 158–165, 2018, doi: 10.1016/j.aca.2018.08.022.

[2] J. Wang *et al.*, “A highly structured hollow ZnO@Ag nanosphere SERS substrate for sensing traces of nitrate and nitrite species in pickled food,” *Sensors Actuators, B Chem.*, vol. 285, no. January, pp. 302–309, 2019, doi: 10.1016/j.snb.2019.01.052.

[3] H. Yang, Y. Xiang, X. Guo, Y. Wu, Y. Wen, and H. Yang, “Diazo-reaction-based SERS substrates for detection of nitrite in saliva,” *Sensors Actuators, B Chem.*, vol. 271, no. November 2017, pp. 118–121, 2018, doi: 10.1016/j.snb.2018.05.111.

[4] R. A. Dweik, “The lung in the balance: Arginine, methylated arginines, and nitric oxide,” *Am. J. Physiol. - Lung Cell. Mol. Physiol.*, vol. 292, no. 1, pp. 2006–2008, 2007, doi: 10.1152/ajplung.00322.2006.

[5] K. H. Kim, S. A. Jahan, and E. Kabir, “A review of breath analysis for diagnosis of human health,” *TrAC - Trends Anal. Chem.*, vol. 33, pp. 1–8, 2012, doi: 10.1016/j.trac.2011.09.013.

[6] B. Buszewski, M. Kesy, T. Ligor, and A. Amann, “Human exhaled air analytics: biomarkers of diseases,” *Biomed. Chromatogr.*, no. 21, pp. 553–566, 2007, doi: 10.1002/bmc.875.

[7] P. B. Jimenez-Vara *et al.*, “Hybrid films of reduced graphene oxide modified with gold nanorods and its study as surface-enhanced Raman spectroscopy platform,” *Mater. Lett.*, vol. 265, p. 127405, 2020, doi: 10.1016/j.matlet.2020.127405.

[8] V. S. Vendamani, S. V. S. N. Rao, A. P. Pathak, and V. R. Soma, “Silicon Nanostructures for Molecular Sensing: A Review,” *ACS Appl. Nano Mater.*, vol. 5, no. 4, pp. 4550–4582, 2022, doi: 10.1021/acsanm.1c04569.

[9] B. Shan, Y. Pu, Y. Chen, M. Liao, and M. Li, “Novel SERS labels: Rational design, functional integration and biomedical applications,” *Coord. Chem. Rev.*, vol. 371, pp. 11–37, 2018, doi: 10.1016/j.ccr.2018.05.007.

[10] E. Singh, M. Meyyappan, and H. S. Nalwa, “Flexible Graphene-Based Wearable

Gas and Chemical Sensors," *ACS Appl. Mater. Interfaces*, vol. 9, no. 40, pp. 34544–34586, 2017, doi: 10.1021/acsami.7b07063.

[11] Π. Α. Ταραντίλης, "Φασματοσκοπία Raman (Raman Spectroscopy) Φασματοσκοπία Raman (Raman Spectroscopy)," vol. 14, no. 12, pp. 3–4, 1988.

[12] M. Righettoni, A. Amann, and S. E. Pratsinis, "Breath analysis by nanostructured metal oxides as chemo-resistive gas sensors," *Mater. Today*, vol. 18, no. 3, pp. 163–171, 2015, doi: 10.1016/j.mattod.2014.08.017.

[13] W. Miekisch, J. K. Schubert, and G. F. E. Noeldge-Schomburg, "Diagnostic potential of breath analysis - Focus on volatile organic compounds," *Clin. Chim. Acta*, vol. 347, no. 1–2, pp. 25–39, 2004, doi: 10.1016/j.cccn.2004.04.023.

[14] N. Emmanuel, R. B. Nair, B. Abraham, and K. Yoosaf, "Fabricating a Low-Cost Raman Spectrometer to Introduce Students to Spectroscopy Basics and Applied Instrument Design," *J. Chem. Educ.*, vol. 98, no. 6, pp. 2109–2116, 2021, doi: 10.1021/acs.jchemed.0c01028.

[15] R. Loudon, "The Raman effect in crystals," *Adv. Phys.*, vol. 50, no. 7 SPEC., pp. 813–864, 2001, doi: 10.1080/00018730110101395.

[16] J. Wu and L. Xie, "Structural Quantification for Graphene and Related Two-Dimensional Materials by Raman Spectroscopy," *Anal. Chem.*, vol. 91, no. 1, pp. 468–481, 2019, doi: 10.1021/acs.analchem.8b04991.

[17] "Renishaw-Raman spectroscopy explained." https://www.renishaw.com/en/raman-spectroscopy-explained--25801.

[18] J. Pérez-Ramírez, G. Mul, and J. A. Moulijn, "In situ Fourier transform infrared and laser Raman spectroscopic study of the thermal decomposition of Co-Al and Ni-Al hydrotalcites," *Vib. Spectrosc.*, vol. 27, no. 1, pp. 75–88, 2001, doi: 10.1016/S0924-2031(01)00119-9.

[19] J. Langer *et al.*, "Present and future of surface-enhanced Raman scattering," *ACS Nano*, vol. 14, no. 1, pp. 28–117, 2020, doi: 10.1021/acsnano.9b04224.

[20] Y. Qiu, C. Kuang, X. Liu, and L. Tang, "Single-Molecule Surface-Enhanced Raman Spectroscopy," *Sensors*, vol. 22, no. 13, pp. 1–16, 2022, doi: 10.3390/s22134889.

[21] M. Fleischmann, P. J. Hendra, and A. J. McQuillan, "Raman spectra of pyridine adsorbed at a silver electrode," *Chem. Phys. Lett.*, vol. 26, no. 2, pp. 163–166, 1974, doi: 10.1016/0009-2614(74)85388.

[22] D. L. Jeanmaire and R. P. VAN Duyne, “Surface Raman Spectroelectrochemistry Part1. Heterocyclic,” *J. Electroanal Chem.*, vol. 84, p. 1, 1977.

[23] H. Kwart and T. J. George, “Q / D,” vol. 4009, no. 1, pp. 5215–5217, 1977.

[24] M. R. Philpott, “Effect of surface Plasmons on transitions in molecules,” *J. Chem. Phys.*, vol. 62, no. 5, pp. 1812–1817, 1975, doi: 10.1063/1.430708.

[25] D. M. Solís, J. M. Taboada, F. Obelleiro, L. M. Liz-Marzán, and F. J. García De Abajo, “Optimization of Nanoparticle-Based SERS Substrates through Large-Scale Realistic Simulations,” *ACS Photonics*, vol. 4, no. 2, pp. 329–337, 2017, doi: 10.1021/acsphotonics.6b00786.

[26] L. Rodríguez-Lorenzo *et al.*, “Zeptomol detection through controlled ultrasensitive surface-enhanced raman scattering,” *J. Am. Chem. Soc.*, vol. 131, no. 13, pp. 4616–4618, 2009, doi: 10.1021/ja809418t.

[27] M. Urbieta *et al.*, “Atomic-Scale Lightning Rod Effect in Plasmonic Picocavities: A Classical View to a Quantum Effect,” *ACS Nano*, vol. 12, no. 1, pp. 585–595, 2018, doi: 10.1021/acsnano.7b07401.

[28] V. Scardaci, “Anisotropic silver nanomaterials by photochemical reactions: Synthesis and applications,” *Nanomaterials*, vol. 11, no. 9, 2021, doi: 10.3390/nano11092226.

[29] W. Fan, Y. H. Lee, S. Pedireddy, Q. Zhang, T. Liu, and X. Y. Ling, “Graphene oxide and shape-controlled silver nanoparticle hybrids for ultrasensitive single-particle surface-enhanced Raman scattering (SERS) sensing,” *Nanoscale*, vol. 6, no. 9, pp. 4843–4851, 2014, doi: 10.1039/c3nr06316j.

[30] S. K. Bhunia, L. Zeiri, J. Manna, S. Nandi, and R. Jelinek, “Carbon-Dot/Silver-Nanoparticle Flexible SERS-Active Films,” *ACS Appl. Mater. Interfaces*, vol. 8, no. 38, pp. 25637–25643, 2016, doi: 10.1021/acsami.6b10945.

[31] Y. Zhou *et al.*, “Ecofriendly and environment-friendly synthesis of size-controlled silver nanoparticles/graphene composites for antimicrobial and SERS actions,” *Appl. Surf. Sci.*, vol. 457, no. July, pp. 1000–1008, 2018, doi: 10.1016/j.apsusc.2018.07.040.

[32] H. Guo, K. Qian, A. Cai, J. Tang, and J. Liu, “Ordered gold nanoparticle arrays on the tip of silver wrinkled structures for single molecule detection,” *Sensors Actuators, B Chem.*, vol. 300, no. July, p. 126846, 2019, doi: 10.1016/j.snb.2019.126846.

[33] Z. Starowicz, R. Wojnarowska-Nowak, P. Ozga, and E. M. Sheregii, “The tuning of the plasmon resonance of the metal nanoparticles in terms of the SERS effect,” *Colloid Polym. Sci.*, vol. 296, no. 6, pp. 1029–1037, 2018, doi: 10.1007/s00396-018-4308-9.

[34] S. Mukherji, S. Bharti, G. Shukla, and S. Mukherji, “Synthesis and characterization of size- And shape-controlled silver nanoparticles,” *Phys. Sci. Rev.*, vol. 4, no. 1, pp. 1–73, 2019, doi: 10.1515/psr-2017-0082.

[35] A. Garcia-Leis, J. V. Garcia-Ramos, and S. Sanchez-Cortes, “Silver nanostars with high SERS performance,” *J. Phys. Chem. C*, vol. 117, no. 15, pp. 7791–7795, 2013, doi: 10.1021/jp401737y.

[36] H. Wang *et al.*, “Transformation from silver nanoprisms to nanodecahedra in a temperature-controlled photomediated synthesis,” *J. Phys. Chem. C*, vol. 116, no. 45, pp. 24268–24273, 2012, doi: 10.1021/jp304941b.

[37] B. Tang, L. Sun, J. Li, M. Zhang, and X. Wang, “Sunlight-driven synthesis of anisotropic silver nanoparticles,” *Chem. Eng. J.*, vol. 260, pp. 99–106, 2015, doi: 10.1016/j.cej.2014.08.044.

[38] W. Cao and Y. Duan, “Current status of methods and techniques for breath analysis,” *Crit. Rev. Anal. Chem.*, vol. 37, no. 1, pp. 3–13, 2007, doi: 10.1080/10408340600976499.

[39] C. Lourenço and C. Turner, “Breath Analysis in Disease Diagnosis: Methodological Considerations and Applications,” *Metabolites*, vol. 4, no. 2, pp. 465–498, 2014, doi: 10.3390/metabo4020465.

[40] J. Kim *et al.*, “Structural Investigation of Chemiresistive Sensing Mechanism in Redox-Active Porous Coordination Network,” *Inorg. Chem.*, vol. 56, no. 15, pp. 8735–8738, 2017, doi: 10.1021/acs.inorgchem.7b01165.

[41] C. Di Natale, R. Paolesse, E. Martinelli, and R. Capuano, “Solid-state gas sensors for breath analysis: A review,” *Anal. Chim. Acta*, vol. 824, pp. 1–17, 2014, doi: 10.1016/j.aca.2014.03.014.

[42] M. A. Correa-Duarte, N. Pazos Perez, L. Guerrini, V. Giannini, and R. A. Alvarez-Puebla, “Boosting the quantitative inorganic surface-enhanced Raman scattering sensing to the limit: The case of nitrite/nitrate detection,” *J. Phys. Chem. Lett.*, vol. 6, no. 5, pp. 868–874, 2015, doi: 10.1021/acs.jpclett.5b00115.

[43] V. Babaahmadi and M. Montazer, “A new route to synthesis silver nanoparticles

on polyamide fabric using stannous chloride," *J. Text. Inst.*, vol. 106, no. 9, pp. 970–977, 2015, doi: 10.1080/00405000.2014.957468.

[44] H. T. Rahal, R. Awad, A. M. Abdel-Gaber, and D. E. S. Bakeer, "Synthesis, Characterization, and Magnetic Properties of Pure and EDTA-Capped NiO Nanosized Particles," *J. Nanomater.*, vol. 2017, 2017, doi: 10.1155/2017/7460323.

[45] K. Saha, S. S. Agasti, C. Kim, X. Li, and V. M. Rotello, "Gold nanoparticles in chemical and biological sensing," *Chem. Rev.*, vol. 112, no. 5, pp. 2739–2779, 2012, doi: 10.1021/cr2001178.

[46] S. Diamai and D. P. S. Negi, "EDTA-capped gold nanoparticles as a colorimetric probe for aluminium," *Mater. Res. Express*, vol. 3, no. 11, 2016, doi: 10.1088/2053-1591/3/11/115002.

[47] A. J. Pereira *et al.*, "Facile Shape-Controlled Fabrication of Copper Nanostructures on Borophosphate Glasses: Synthesis, Characterization, and Their Highly Sensitive Surface-Enhanced Raman Scattering (SERS) Properties," *J. Phys. Chem. C*, vol. 120, no. 22, pp. 12265–12272, 2016, doi: 10.1021/acs.jpcc.6b02881.

[48] J. Tang *et al.*, "Wrinkled Ag nanostructured gratings towards single molecule detection by ultrahigh surface Raman scattering enhancement," *Sensors Actuators, B Chem.*, vol. 218, pp. 145–151, 2015, doi: 10.1016/j.snb.2015.04.008.

[49] G. Macias, M. Alba, L. F. Marsal, and A. Mihi, "Surface roughness boosts the SERS performance of imprinted plasmonic architectures," *J. Mater. Chem. C*, vol. 4, no. 18, pp. 3970–3975, 2016, doi: 10.1039/c5tc02779a.

[50] S. B. Chaney, S. Shanmukh, and R. A. Dluhy, "Polarized Surface Enhanced Raman and Absorbance Spectra of Aligned Silver Nanorod Arrays," *J. Phys. Chem. B*, no. 110, pp. 3153–3157, 2006.

[51] M. Chen, H. Zhang, Y. Ge, S. Yang, P. Wang, and Y. Fang, "Surface-Nanostructured Single Silver Nanowire: A New One-Dimensional Microscale Surface-Enhanced Raman Scattering Interface," *Langmuir*, vol. 34, no. 50, pp. 15160–15165, 2018, doi: 10.1021/acs.langmuir.8b02854.

[52] L. Polavarapu and Q. H. Xu, "Water-soluble conjugated polymer-induced self-assembly of gold nanoparticles and its application to SERS," *Langmuir*, vol. 24,

no. 19, pp. 10608–10611, 2008, doi: 10.1021/la802319c.

[53] T. V. Vineesh, V. Yarmiayev, and D. Zitoun, “Tailoring the electrochemical hydrogen evolution activity of Cu3P through oxophilic surface modification,” *Electrochem. commun.*, vol. 113, no. December 2019, p. 106691, 2020, doi: 10.1016/j.elecom.2020.106691.

[54] S. Chen, X. Li, Y. Guo, and J. Qi, “A Ag-molecularly imprinted polymer composite for efficient surface-enhanced Raman scattering activities under a low-energy laser,” *Analyst*, vol. 140, no. 9, pp. 3239–3243, 2015, doi: 10.1039/c4an02301c.

[55] W. Xu *et al.*, “Surface enhanced Raman spectroscopy on a flat graphene surface,” *Proc. Natl. Acad. Sci. U. S. A.*, vol. 109, no. 24, pp. 9281–9286, 2012, doi: 10.1073/pnas.1205478109.

[56] C. Hu *et al.*, “Fabrication of a graphene oxide-gold nanorod hybrid material by electrostatic self-assembly for surface-enhanced Raman scattering,” *Carbon N. Y.*, vol. 51, no. 1, pp. 255–264, 2013, doi: 10.1016/j.carbon.2012.08.051.

[57] R. Tong, X. Hu, G. Fang, S. Sun, J. Liu, and S. Wang, “Rapid detection of hexamethylenetetramine based on the substrate UC@SiO2@Au@Ag using SERS,” *RSC Adv.*, vol. 7, no. 79, pp. 49969–49974, 2017, doi: 10.1039/c7ra07634g.

[58] B. Küstner *et al.*, “SERS labels for red laser excitation: Silica-encapsulated SAMs on tunable gold/silver nanoshells,” *Angew. Chemie - Int. Ed.*, vol. 48, no. 11, pp. 1950–1953, 2009, doi: 10.1002/anie.200804518.

[59] L. Zhang *et al.*, “Sensitive Detection of Rhodamine B in Condiments Using Surface-Enhanced Resonance Raman Scattering (SERRS) Silver Nanowires as Substrate,” *Appl. Spectrosc.*, vol. 71, no. 10, pp. 2395–2403, 2017, doi: 10.1177/0003702817711700.

[60] Z. Li, M. Li, C. Wang, X. Zhou, J. Li, and D. Li, “Highly sensitive and selective method for detection of trace amounts of nitrite in aquaculture water by SERRS coupled with diazo reaction,” *Sensors Actuators, B Chem.*, vol. 297, no. July, p. 126757, 2019, doi: 10.1016/j.snb.2019.126757.

[61] X. X. Han, P. Pienpinijtham, B. Zhao, and Y. Ozaki, “Coupling reaction-based ultrasensitive detection of phenolic estrogens using surface-enhanced resonance raman scattering,” *Anal. Chem.*, vol. 83, no. 22, pp. 8582–8588, 2011, doi:

10.1021/ac2019766.

[62] T. K. Sau and C. J. Murphy, “Room temperature, high-yield synthesis of multiple shapes of gold nanoparticles in aqueous solution,” *J. Am. Chem. Soc.*, vol. 126, no. 28, pp. 8648–8649, 2004, doi: 10.1021/ja047846d.

[63] M. Kim, H. J. Park, S. W. Han, J. Park, and W. S. Yun, “Shape transformation of gold nanoparticles from octahedron to cube depending on in situ seed-growth time,” *Bull. Korean Chem. Soc.*, vol. 34, no. 8, pp. 2243–2244, 2013, doi: 10.5012/bkcs.2013.34.8.2243.

[64] J. P. Sylvestre, S. Poulin, A. V. Kabashin, E. Sacher, M. Meunier, and J. H. T. Luong, “Surface chemistry of gold nanoparticles produced by laser ablation in aqueous media,” *J. Phys. Chem. B*, vol. 108, no. 43, pp. 16864–16869, 2004, doi: 10.1021/jp047134.

[65] L. Váradi, M. Breedon, F. F. Chen, A. Trinchi, I. S. Cole, and G. Wei, “Evaluation of novel Griess-reagent candidates for nitrite sensing in aqueous media identified via molecular fingerprint searching,” *RSC Adv.*, vol. 9, no. 7, pp. 3994–4000, 2019, doi: 10.1039/c8ra07656a.

[66] W. Ahmad *et al.*, “Design of Physicochemical Factors for Regulating the Retention Mechanism of 4-Aminothiophenol in Surface-Enhanced Raman Scattering toward Nitrite Sensing,” *J. Phys. Chem. C*, vol. 124, no. 14, pp. 7768–7776, 2020, doi: 10.1021/acs.jpcc.9b11295.

[67] Z. Xu, Z. Liang, W. Guo, and R. Zou, “In situ/operando vibrational spectroscopy for the investigation of advanced nanostructured electrocatalysts,” *Coord. Chem. Rev.*, vol. 436, p. 213824, 2021, doi: 10.1016/j.ccr.2021.213824.

[68] R. Pilot, R. Signorini, C. Durante, L. Orian, M. Bhamidipati, and L. Fabris, “A review on surface-enhanced Raman scattering,” *Biosensors*, vol. 9, no. 2, 2019, doi: 10.3390/bios9020057.

[69] S. Feng *et al.*, “Ultrasensitive molecular sensor using N-doped graphene through enhanced Raman scattering,” *Sci. Adv.*, vol. 2, no. 7, pp. 1–12, 2016, doi: 10.1126/sciadv.1600322.

[70] B. Li, Z. Tian, H. Li, Z. Yang, Y. Wang, and X. Wang, “Self-supporting graphene aerogel electrode intensified by NiCo2S4 nanoparticles for asymmetric supercapacitor,” *Electrochim. Acta*, vol. 314, pp. 32–39, 2019, doi: 10.1016/j.electacta.2019.05.040.

[71] W. Liu *et al.*, “Construction of ultra-sensitive surface-enhanced Raman scattering substrates based on 3D graphene oxide aerogels,” *Carbon N. Y.*, vol. 202, no. P1, pp. 389–397, 2023, doi: 10.1016/j.carbon.2022.11.001.

[72] Y. K. Kim, S. W. Han, and D. H. Min, “Graphene oxide sheath on ag nanoparticle/graphene hybrid films as an antioxidative coating and enhancer of surface-enhanced raman scattering,” *ACS Appl. Mater. Interfaces*, vol. 4, no. 12, pp. 6545–6551, 2012, doi: 10.1021/am301658p.

[73] Y. Matsumoto *et al.*, “Photoreaction of graphene oxide nanosheets in water,” *J. Phys. Chem. C*, vol. 115, no. 39, pp. 19280–19286, 2011, doi: 10.1021/jp206348s.

[74] A. Ganguly, S. Sharma, P. Papakonstantinou, and J. Hamilton, “Probing the thermal deoxygenation of graphene oxide using high-resolution in situ X-ray-based spectroscopies,” *J. Phys. Chem. C*, vol. 115, no. 34, pp. 17009–17019, 2011, doi: 10.1021/jp203741y.